ATTACHMENT 25

Browns Ferry Nuclear Plant (BFN)
Unit 1

Technical Specifications (TS) Change 473

AREVA Fuel Transition

Applicability of AREVA NP BWR Methods to Extended Power Uprate Conditions
(Non-Proprietary)

Attached is the non-proprietary version of a report prepared by AREVA discussing the applicability of approved licensing analysis methods to extended power uprate conditions.

L32 091009 801

An AREVA and Siemens company

ANP-2638NP
Revision 2

Applicability of AREVA NP BWR Methods to Extended Power Uprate Conditions

October 2009

AREVA

AREVA NP Inc.

ANP-2638NP
Revision 2

Applicability of AREVA NP BWR Methods to Extended Power Uprate Conditions

Copyright © 2009

AREVA NP Inc.
All Rights Reserved

Nature of Changes

Item	Page	Description and Justification
1.	B-7	Updated Figure B-1.

Contents

1.0 Introduction 1-1

2.0 Overview 2-1

3.0 Thermal-Hydraulics 3-1

4.0 SPCB CHF Correlation 4-1

5.0 Safety Limit MCPR 5-1

6.0 Mechanical Limits Methodology 6-1

7.0 Core Neutronics 7-1

8.0 Transient Analysis 8-1

9.0 LOCA Analysis 9-1

10.0 Stability Analysis 10-1

11.0 Summary 11-1

12.0 References 12-1

Appendix A Application of AREVA NP Methodology for Mixed Cores A-1

A.1 Discussion A-1

A.2 References A-5

Appendix B Thermal Hydraulic Methods B-1

B.1 Hydraulic Characterization B-1

B.2 References B-5

Appendix C Neutronic Methods C-1

C.1 Cross Section Representation C-1

C.2 Applicability of Uncertainties C-5

C.3 Fuel Cycle Comparisons C-10

C.3.1 Bypass Voiding C-12

C.3.2 Fuel Assembly Design C-14

C.4 References C-14

Appendix D Stability Methods D-1

D.1 DIVOM Analysis D-1

D.2 ATWS/Instability D-1

D.2.1 Background D-2

D.2.2 Review of the Important Phenomena D-3

D.2.2.1 Global Oscillation Limit Cycle Amplitude D-3

D.2.2.2 Average Power Increase due to Oscillations D-4

D.2.2.3 Limiting Mode D-5

D.2.2.4 The Role of the Prompt-Critical Pulses D-5

D.2.2.5 The Role of Void-Reactivity Coefficient D-6

D.2.3 Assessing the Change in Fuel Damage Potential D-6

D.2.3.1 Effect of the ATRIUM-10 Fuel Type D-7

D.2.3.2 Effect of EPU Core Loading D-7

D.3 References D-8

Tables

Table 7-1 CASMO-4/MICROBURN-B2 Operating Experience 7-2

Table B-1 AREVA NP Multi-Rod Void Fraction Validation Database B-6

Table C-1 KWU-S Gamma Scan Benchmark Results from EMF-2158(P)(A) C-15

Table C-2 Comparison of CASMO-4 and MCNP results for ATRIUM-10 Design C-15

Table C-3 Fuel Enrichment Description for the Initial Browns Ferry Unit 1 EPU ATRIUM-10 Fuel Cycle Design C-16

Figures

Figure 3-1 Comparison of Karlstein Two-Phase Pressure Drop Test Matrix and Typical Reactor Conditions 3-2

Figure 5-1 Assembly Power Distribution for Limiting Case in Safety Limit MCPR Analysis 5-4

Figure 8-1 Typical Hydraulic Benchmarks to Karlstein Transient Simulations 8-3

Figure B-1 Comparison of the Measured Local Quality for ATRIUM-10 Void Data and Exit Quality for Typical Reactor Conditions B-7

Figure B-2 Validation of [ ] using FRIGG-2 and FRIGG-3 Void Data B-7

Figure B-3 Validation of [ ] using ATRIUM-10 Void Data B-8

Figure B-4 Validation of Ohkawa-Lahey using FRIGG-2 and FRIGG-3 Void Data B-8

Figure B-5 Validation of Ohkawa-Lahey using ATRIUM-10 Void Data B-9

Figure B-6 Measured Versus Calculated Void Fractions B-910

Figure C-1 Microscopic Thermal Cross Section of U-235 from Base Depletion and Branches C-17

Figure C-2 Microscopic Fast Cross Section of U-235 from Base Depletion and Branches C-17

Figure C-3 Microscopic Thermal Cross Section of U-235 at Beginning of Life C-18

Figure C-4 Microscopic Fast Cross Section of U-235 at Beginning of Life C-18

Figure C-5 Microscopic Thermal Cross Section of U-235 Comparison of Quadratic Fit with Explicit Calculations at Various Void Fractions C-19

Figure C-6 Microscopic Fast Cross Section of U-235 Comparison of Quadratic Fit with Explicit Calculations at Various Void Fractions C-19

Figure C-7 Macroscopic Diffusion Coefficient (Fast and Thermal) Comparison of Quadratic Fit with Explicit Calculations at Various Void Fractions C-20

Figure C-8 Microscopic Thermal Cross Section of U-235 at 70 GWd/MTU C-21

Figure C-9 Quadratic Interpolation Illustration of Microscopic Thermal Cross Section of U-235 ..... C-22

Figure C-10 Illustration of Final Quadratic Interpolation for Microscopic Thermal Cross Section of U-235 ..... C-22

Figure C-11 Comparison of k-infinity from MICROBURN-B2 Interpolation Process with CASMO-4 Calculations at Intermediate Void Fractions of 0.2, 0.6 and 0.9 ..... C-23

Figure C-12 Comparison of k-infinity from MICROBURN-B2 Interpolation Process with CASMO-4 Calculations at 0.4 Historical Void Fractions and 0.9 Instantaneous Void Fraction C-23

Figure C-13 Delta k-infinity from MICROBURN-B2 Interpolation Process with CASMO-4 Calculations at 0.4 Historical Void Fraction and 0.9 Instantaneous Void Fraction C-24

Figure C-14 Comparison of Interpolation Process Using Void Fractions of 0.0, 0.4 and 0.8 and Void Fractions of 0.0, 0.45 and 0.9 ..... C-24

Figure C-15 PU-239 sigma-1 Dependence on Spectral History at 20 GWd/T C-25

Figure C-16 PU-240 sigma-1 Dependence on Spectral History at 20 GWd/T C-25

Figure C-17 EMF-2158(P)(A) TIP Statistics by Axial Level C-26

Figure C-18 Quad Cities Unit 1 Pin by Pin Gamma Scan Results C-26

Figure C-10 Maximum Assembly Power in Topical Report EMF-2158(P)(A) C-27

Figure C-20 Maximum Exit Void Fraction in Topical Report EMF-2158(P)(A) C-27

Figure C-21 Maximum Assembly Power Observed from Recent Operating Experience C-28

Figure C-22 Void Fractions Observed from Recent Operating Experience C-28

Figure C-23 Axial Power and Void Profile Observed from Recent Design Experience C-29

Figure C-24 Nodal Void Fraction Histogram Observed from Recent Design Experience C-29

Figure C-25 Maximum Assembly Power in an EPU Browns Ferry Design C-30

Figure C-26 Maximum Exit Void Fraction in an EPU Browns Ferry Design C-30

Figure C-27 Browns Ferry EPU Design Axial Profile of Power and Void Fraction C-31

Figure C-28 Browns Ferry EPU Design Nodal Void Fraction Histogram C-31

Figure C-29 Hypothetical MICROBURN-B2 Multi-Channel Average Bypass Void Distribution C-32

This document contains a total of 86 pages

Nomenclature

Acronym	Definition
BWR	Boiling Water Reactor
CHF	Critical Heat Flux
EPU	Extended Power Uprate
LHGR	Linear Heat Generation Rate
LOCA	Loss of Coolant Accident
LRNB	Load Reject with no Bypass
MAPLHGR	Maximum Average Planar Linear Heat Generation Rate
MCPR	Minimum Critical Power Ratio
NRC	Nuclear Regulatory Commission
OLMCPR	Operating Limit Minimum Critical Power Ratio
RAI	Request for Additional Information
SER	Safety Evaluation Report
SLMCPR	Safety Limit Minimum Critical Power Ratio

1.0 Introduction

This document reviews the AREVA NP* licensing methodologies to demonstrate that they are applicable to operation of the Browns Ferry Nuclear Power Generating Stations at Extended Power Uprate (EPU) conditions. EPU conditions refer to power uprate to 120% of the originally licensed rated thermal power.

* AREVA NP Inc. is an AREVA and Siemens company.

2.0 Overview

The first step in determining the applicability of current licensing methods to EPU conditions was a review of current AREVA NP BWR topical reports to identify SER restrictions on the BWR methodology. This review identified that there are no SER restrictions on power level for the AREVA NP topical reports. The review also indicated that there are no SER restrictions on the parameters most impacted by the increased power level: steam flow, feedwater flow, jet pump M-ratio, and core average void fraction.

The second step consisted of an evaluation of the core and reactor conditions experienced under EPU conditions to determine any challenges to the validity of the models. When the reactor power is increased, the resultant impact on operating margin is mitigated to a large extent by a decrease in the limiting assembly radial power factor. This decrease in the limiting assembly radial power factor is necessary since the thermal operating limits (MCPR, MAPLHGR and LHGR) that restrict assembly power are dependent on the limiting assembly power but are fairly insensitive to the core thermal power. From this fundamental constraint the following observations may be made about the EPU operating conditions:

1. The reduction in the hot assembly radial peaking factor leads to a more uniform radial power distribution and consequently a more uniform core flow distribution. The net result being less flow starvation of the hottest assemblies.
2. With the flatter radial power distribution, more assemblies and fuel rods are near thermal limits.
3. From a system perspective, there will be higher steam flow and feedwater flow rates.
4. With an increase in the average assembly power in the reactor, the core pressure drop will increase slightly resulting in a decrease in the jet pump M-ratio for a given core flow rate.
5. Core average void fraction will increase.

Based on these fundamental characteristics of power uprate, each of the major analysis domains (thermal-hydraulics, core neutronics, transient analysis, LOCA and stability) are assessed to determine any challenges to EPU application. A description of the analyses performed for a transition cycle is provided in Appendix A.

3.0 Thermal-Hydraulics

AREVA NP assembly thermal-hydraulic methods are qualified and validated against full-scale heated bundle tests in the KATHY test facility in Karlstein, Germany. The KATHY tests are used to characterize the assembly two-phase pressure drop and CHF performance. This allows the hydraulic models to be verified for AREVA NP fuel designs over a wide range of hydraulic conditions prototypic of reactor conditions.

The standard matrix of test conditions for KATHY is compared to reactor conditions in Figure 3-1. This figure illustrates that the test conditions bound uprated assembly conditions. These tests were performed on the same ATRIUM™-10* fuel assembly that is to be loaded in the Browns Ferry core. The Browns Ferry data is based upon the projected uprated conditions. Figure 3-1 also shows that the key physical phenomena (e.g. heat flux, fluid quality and assembly flows) for uprated conditions are within the scope of and bounded by current reactor experience.

This similarity of assembly conditions is further enforced in AREVA NP analysis methodologies by the imposition of SPCB CHF correlation limits and therefore both current designs and uprated designs must remain within the same parameter space. Since the bundle operating conditions for EPU are within the envelope of hydraulic test data used for model qualification and operating experience, the hydraulic models used to compute the core flow distribution and local void content remain valid for EPU conditions.

A more detailed discussion about the thermal hydraulic analyses is presented in Appendix B.

* ATRIUM™-10 is a trademark of AREVA NP Inc.

Figure 3-1 Comparison of Karlstein Two-Phase Pressure Drop Test Matrix and Typical Reactor Conditions

4.0 SPCB CHF Correlation

The SPCB CHF correlation (Reference 7) was approved by the NRC staff to be applicable over specified ranges of mass flow, pressure, inlet subcooling, and boiling transition enthalpy. The NRC staff also approved specific corrective actions when the computed conditions fall outside of the approved range to assure that conservative calculations are obtained (Table 4.1). For both EPU and pre-EPU conditions, some analyses can predict assembly conditions to be outside the approved range of specified conditions for the CHF correlations. Consequently, the AREVA NP licensing methods are programmed to determine whether the computed assembly conditions fall outside of the approved range of applicability for the CHF correlation; if so, the methodology imposes approved corrective actions to conservatively assess the critical power margin for the assembly. The critical power correlation methodology for co-resident fuel is presented in Reference 12 and discussed in Appendix A

Table 4.1 Bounds Checking

5.0 Safety Limit MCPR

The safety limit MCPR (SLMCPR) methodology is used to determine the Technical Specification SLMCPR value that ensures that 99.9% of the fuel rods are expected to avoid boiling transition during normal reactor operation and anticipated operation occurrences. The SLMCPR methodology is described in Reference 1. The SLMCPR is determined by statistically combining calculation uncertainties and plant measurement uncertainties that are associated with the calculation of MCPR. The thermal hydraulic, neutronic, and critical power correlation methodologies are used in the calculation of MCPR. The applicability of these methodologies for EPU conditions is discussed in other sections of this report. As discussed in Section 2.0, EPU operation will result in a flatter radial power distribution with more fuel rods operating near thermal limits. This is the most significant impact of EPU operation on the SLMCPR calculation and is explicitly accounted for in the methodology as discussed below.

AREVA NP calculates the SLMCPR on a cycle-specific basis to protect all allowed reactor operating conditions. The analysis incorporates the cycle-specific fuel and core designs. The initial MCPR distribution of the core is a major factor affecting how many rods are predicted to be in boiling transition. The MCPR distribution of the core depends on the neutronic design of the reload fuel and the fuel assembly power distributions in the core. AREVA NP SLMCPR methodology specifies that analyses be performed with a design basis power distribution that "... conservatively represents expected reactor operating states which could both exist at the MCPR operating limit and produce a MCPR equal to the MCPR safety limit during an anticipated operational occurrence." (Reference 1, Section 5.0).

[

]

[

]

The impact that a flatter core power distribution may have on the SLMCPR is explicitly accounted for by the methodology. EPU operation will lead to a flatter core power distribution; [

]

Control rod patterns are not a direct input to the SLMCPR analysis; the primary impact of control rod patterns is on the power distribution used in the SLMCPR analysis. [

] The power distributions considered in the SLMCPR analysis reflect the control rod patterns planned for the range of core flow expected at EPU rated power during the entire cycle.

The primary impact of ARTS/MELLLA operation on the SLMCPR analysis is the lower minimum allowed core flow at rated power. Licensing analyses performed by AREVA NP recognize that SLMCPR is dependent on core flow. [ ]

[

]

Figure 5-1 Assembly Power Distribution for Limiting Case in Safety Limit MCPR Analysis

6.0 Mechanical Limits Methodology

The LHGR limit is established to support plant operation while satisfying the fuel mechanical design criteria. The LHGR limit is translated into power history inputs as described in the Reference 2 topical report (see the response to RAI, Question 3, in Reference 2). Then, the power histories are used as input to the RODEX2A, RAMPEX and COLAPX codes in evaluating the fuel rod thermal-mechanical criteria (References 3, 4, and 14).

Higher voiding, associated with EPU operation, can have the effect of further offsetting the axial power and fast neutron flux profiles during operation. Because the power history methodology makes use of established axial profiles, changes to the power history due to higher voiding are not explicitly taken into account in the analyses. However, the profiles selected for the analyses are conservatively peaked to result in higher rod average power levels while attaining the LHGR limit. Separate studies (Reference 6) have shown the current methodology, which makes use of a bounding power history, to be conservative for EPU conditions.

7.0 Core Neutronics

The AREVA NP neutronic methodologies (References 15 and 17) are characterized by technically rigorous treatment of phenomena and are very well benchmarked (>100 cycles of operation plus gamma scan data for ATRIUM-10). Recent operating experience is tabulated in Table 7-1. This table presents the reactor operating conditions and in particular the average and hot assembly powers for both US and European applications. As can be seen from this information, the average and peak bundle powers in this experience base exceed that associated with the power uprate for Browns Ferry.

The increased steam flow from power uprate comes from increased power in normally lower power assemblies in the core, operating at higher power levels. High powered assemblies in uprated cores will be subject to the same LHGR, MAPLHGR, MCPR, and cold shutdown margin limits and restrictions as high powered assemblies in non-uprated cores.

The similarity of operating conditions between current and uprate conditions assures that the neutronic methods used to compute the nodal reactivity and power distributions remain valid. Furthermore, the neutronic characteristics computed by the steady-state simulator and used in safety analysis remain valid.

Detailed analysis of the neutronic methodology and its specific applicability to Browns Ferry is presented in Appendix C.

Table 7-1 CASMO-4/MICROBURN-B2 Operating Experience

Reactor	Reactor Size, #FA	Power, MWt (% Uprated)*	Ave. Bundle Power, MWt/FA	Approximate Peak Bundle Power, MWt/FA	Fuel/Cycle Licensing**	Uprate Comments
A	592	2575 (0.0)	4.4	7.2	X	
B	592	2575 (0.0)	4.4	7.4	X	
C	532	2292 (0.0)	4.3	7.3	(X)	
D	840	3690 (0.0)	4.4	7.5	X	Licensing only through Cycle 20
E	500	2500 (15.7)	5.0	8.0	X	For 3 cycles oper.
F	444	1800 (5.9)	4.1	7.3	X	
G	676	2928 (8.0)	4.3	7.6	(X)	
H	700	3300 (9.3)	4.7	8.0	(X)	
I	784	3840 (0.0)	4.9	8.1	(X)	
J	624	3237 (11.9)	5.2	7.8	(X)	
K	648	3600 (14.7)	5.6	8.6	(X)	With ATRIUM-10XM
L	648	2500 (10.1)	3.9	6.9	(X)	
M	624	3091 (6.7)	5.0	7.7	X	
N	800	3898 (1.7)	4.9	7.7	X	
O	764	3489 (5.0)	4.6	7.2	X	
P	560	2923 (20)	5.2	8.0	X	
Q	764	3952 (20)	5.2	7.7	X	
Browns Ferry 1/2/3†	764	3952 (20.0)	5.2	7.7	none	EQ cycle study

* Latest power uprates.
** (x)=currently fuel licensing only (Europe).
† Browns Ferry added for comparison purposes only, i.e., not in the Operating Experience database.

8.0 Transient Analysis

The AREVA transient analysis methodology is described in References 9, 10, 11, and 16. The core phenomena of primary interest for limiting transients in BWRs are void fraction/quality relationships, determination of CHF, pressure drop, reactivity feedbacks and heat transfer correlations. One fundamental validation of the core hydraulic solution is separate effects testing against Karlstein transient CHF measurements. The transient benchmark to time of dryout for prototypic Load Reject with no Bypass (LRNB) and pump trip transients encompass the transient integration of the continuity equations (including the void-quality closure relation), heat transfer, and determination of CHF. Typical benchmarks to Karlstein (Figure 8-1) illustrate that the transient hydraulic solution and application of SPCB result in conservative predictions of the time of dryout. The measured data is taken from ATRIUM-10 tests.

Outside of the core, the system simulation relies primarily on solutions of the basic conservation equations and equations of state. While there are changes to the feedwater flow rate and jet pump M-ratio associated with power uprate, the most significant change is the steam flow rate and the associated impact on the steamline dynamics for pressurization events. The models associated with predicting the pressure wave are general and have no limitation within the range of variation associated with power uprate.

The reactivity feedbacks are validated by a variety of means including initial qualification of advanced fuel design lattice calculations to Monte Carlo results as required by SER restrictions, steady-state monitoring of reactor operation (power distributions and eigenvalue), and the Peach Bottom 2 turbine trip benchmarks that exhibited a minimum of 3.8% conservatism in the calculation of integral power.

From these qualifications and the observation that the nodal hydraulic conditions during EPU are expected to be within the current operating experience, the transient analysis methods remain valid.

AREVA NP performs ATWS analysis to demonstrate compliance with the peak pressurization criteria which occurs very early in the transient. The early system response during an ATWS event is essentially the same as a transient event and the same code is used to calculate the

system response. The impact of EPU operation on the ATWS peak pressure analysis is the same as in the transient analysis system response.

Figure 8-1 Typical Hydraulic Benchmarks to Karlstein Transient Simulations

9.0 LOCA Analysis

The MAPLHGR is generally selected to be slightly less restrictive than the LHGR limit. The adequacy of the selected MAPLHGR limit is demonstrated by performing analyses to confirm that all 10 CFR 50.46 acceptance criteria are satisfied during a postulated LOCA. If all acceptance criteria are not satisfied, a more restrictive MAPLHGR limit is selected.

LOCA results are strongly dependent on local power and are weakly dependent on core average power. As discussed in previous sections, maximum local power is not significantly changed due to power uprate because the core is still constrained by the same thermal limits. The parameters associated with power uprate that may impact LOCA results are: increased core average initial stored energy, decreased initial coolant inventory, relative flow distribution between highest power and average power assemblies, and increased core decay heat. The AREVA methodology applicable to LOCA is described in References 5 and 13.

BWR LOCA analyses are not sensitive to initial stored energy. During the blowdown phase the heat transfer remains high and the stored energy is removed prior to the start of the heatup phase. Initial inventory differences may impact LOCA event timing and the minimum inventory during blowdown prior to refill of the reactor vessel. However, any impact on event timing or minimum inventory would be smaller than the impact associated with the different size breaks that are already considered in the break spectrum analyses. At EPU conditions, the difference in flow between the highest power assembly and the average power assembly is reduced relative to pre-EPU conditions. Therefore, these parameters do not change the range of conditions encountered or the capability of the codes to model LOCA at EPU conditions.

The potential impact of power uprate on LOCA analyses is thus primarily associated with the increase in decay heat levels in the core. Decay heat is conservatively modeled using industry standards applied as specified by regulatory requirements. The models used for decay heat calculations are valid for EPU.

High void fractions occur during the blowdown, refill, and reflood phases of a LOCA. The thermal hydraulic models used in the LOCA Appendix K evaluation model (Reference 5) are appropriate for the range of void conditions encountered during a LOCA. Initial fuel rod local peaking factors are calculated for void characteristics representative for reactor conditions prior

to the start of the accident. The effect of initial void on local peaking factor is less important than the lattice designs and exposure ranges considered in the analysis.

From the above discussion and the observation that nodal thermal-hydraulic conditions during EPU are expected to be within the current operating experience, the LOCA methods remain applicable for EPU conditions.

The Appendix R analysis is performed using the approved LOCA analysis codes. Similar to LOCA events, the impact of power uprate on the Appendix R analysis is primarily associated with the increase in decay heat in the core. Decay heat is conservatively modeled using industry standards. Use of the Appendix K heat transfer correlations and logic is conservative for Appendix R calculations.

The Browns Ferry LOCA analyses performed for Units 2 and 3 are also applicable for Unit 1 since the core operational conditions, modeled geometry and ECCS parameters are identical. A review of geometry between Units 1, 2 and 3 determined the only significant difference was the recirculation piping for Unit 3 (Unit 3 has undergone a recirculation header and riser replacement). The differences in recirculation piping for Unit 3 does not result in any modifications to recirculation piping model used in the LOCA analyses (the simplications of the recirculation piping model does not distinguish the differences). Refer to Appendix A for the application of AREVA NP LOCA analyses for mixed cores.

10.0 Stability Analysis

The flatter radial power profile induced by the power uprate will tend to decrease the first azimuthal eigenvalue separation and result in slightly higher regional decay ratios. These effects are computed by STAIF as it directly computes the channel, global, and regional decay ratio and does not rely on a correlation to protect the regional mode.

STAIF has been benchmarked against full assembly tests (in KATHY facility) to validate the channel hydraulics from a decay ratio of approximately 0.4 to limit cycles. These tests or benchmarks exceed the bounds of EPU operation. These benchmarks include prototypical ATRIUM-10 assemblies. From a reactor perspective, STAIF is benchmarked to both global and regional reactor data as late as 1998, and therefore includes current reactor cycle and fuel design elements. This strong benchmarking qualification and the direct computation of the regional mode assure that the impact of the "flatter" core design for power uprate will be reflected in the stability analysis.

Detailed analysis of the stability methodology and it's specific applicability to Browns Ferry are presented in Appendix D.

11.0 Summary

This review concluded that there are no SER restrictions on AREVA NP methodology that are impacted by EPU. Since the EPU core and assembly conditions for the Browns Ferry units are equivalent to core and assembly conditions of other plants for which the methodology was benchmarked, the AREVA NP methodology (including uncertainties) remains applicable for EPU conditions at the Browns Ferry Units.

More specifically:

a) The steady state and transient neutronics and thermal-hydraulic analytical methods and code systems supporting EPU are within NRC approved applicability ranges because the conditions for EPU application are equivalent to existing core and assembly conditions in other plants for which the AREVA NP methodology was benchmarked.

b) The calculational and measurement uncertainties applied in EPU applications are valid because the conditions for EPU application are equivalent to existing core and assembly conditions for which the AREVA NP methodology was benchmarked.

c) The assessment database and uncertainty of models used to simulate the plant response at EPU conditions are equivalent to core and assembly conditions for which the AREVA NP methodology was benchmarked.

12.0 References

1. ANF-524(P)(A) Revision 2 and Supplements 1 and 2, "ANF Critical Power Methodology for Boiling Water Reactors," Advanced Nuclear Fuels Corporation, November 1990.

2. XN-NF-85-67(P)(A) Revision 1, "Generic Mechanical Design for Exxon Nuclear Jet Pump BWR Reload Fuel," Exxon Nuclear Company, September 1986.

3. ANF-89-98(P)(A) Revision 1 and Supplement 1, "Generic Mechanical Design Criteria for BWR Fuel Designs," Advanced Nuclear Fuels Corporation, May 1995.

4. EMF-85-74(P) Revision 0, Supplement 1(P)(A) and Supplement 2(P)(A), "RODEX2A (BWR) Fuel Rod Thermal-Mechanical Evaluation Model," Siemens Power Corporation, February 1998.

5. EMF-2361(P)(A), "EXEM BWR-2000 ECCS Evaluation Model," Framatome ANP, May 2001.

6. BAW-10247PA Revision 1 and Supplement 1, "Realistic Thermal-Mechanical Fuel Rod Methodology for Boiling Water Reactors," AREVA NP Inc., April 2008.

7. EMF-2209(P)(A) Revision 2, *SPCB Critical Power Correlation*, Framatome ANP, September 2003.

8. XN-NF-80-19(P)(A) Volume 3 Revision 2, "Exxon Nuclear Methodology for Boiling Water Reactors, THERMEX: Thermal Limits Methodology Summary Description," Exxon Nuclear Company, January 1987.

9. XN-NF-84-105(P)(A) Volume 1 and Volume 1 Supplements 1 and 2, Revision 1, "XCOBRA-T: A computer Code for BWR Transient Thermal-Hydraulic Core Analysis," Exxon Nuclear Company, February 1987.

10. ANF-913(P)(A) Volume 1 Revision 1 and Volume 1 Supplements 2, 3, and 4, "COTRANSA2: A Computer Program for Boiling Water Reactor Transient Analyses," Advanced Nuclear Fuels Corporation, August 1990.

11. ANF-1358(P)(A) Revision 3, "The Loss of Feedwater Heating Transient in Boiling Water Reactors," Framatome ANP, September 2005.

12. EMF-2245(P)(A) Revision 0, "Application of Siemens Power Corporation's Critical Power Correlations to Co-Resident Fuel," Siemens Power Corporation, August 2000.

13. EMF-2292(P)(A) Revision 0, "ATRIUM™-10: Appendix K Spray Heat Transfer Coefficients," Siemens Power Corporation, September 2000.

14. XN-NF-81-58(P)(A) Revision 2 and Supplements 1 and 2, "RODEX2 Fuel Rod Thermal-Mechanical Response Evaluation Model," Exxon Nuclear Company, March 1984.

15. XN-NF-80-19(P)(A) Volume 1 and Supplements 1 and 2, "Exxon Nuclear Methodology for BWR Water Reactors – Neutronic Methods for Design and Analysis," Exxon Nuclear Company, March 1983.

16. XN-NF-80-19(P)(A) Volume 4 Revision 1, "Exxon Nuclear Methodology for BWR Water Reactors: Application of the ENC Methodology to BWR Reloads," Exxon Nuclear Company, June 1986.

17. EMF-2158(P)(A) Revision 0, "Siemens Power Corporation Methodology for Boiling Water Reactors: Evaluation and Validation of CASMO-4/MICROBURN-B2," Siemens Power Corporation, October 1999.

Appendix A Application of AREVA NP Methodology for Mixed Cores

A.1 Discussion

AREVA NP has considerable experience analyzing fuel design transition cycles and has methodology and procedures to analyze mixed cores composed of multiple fuel types. For each core design, analyses are performed to confirm that all design and licensing criteria are satisfied. The analyses performed explicitly include each fuel type in the core. The analyses consider the cycle-specific core loading and use input data appropriate for each fuel type in the core. The mixed core analyses are performed using generically approved methodology in a manner consistent with NRC approval of the methodology. Based on results from the analyses, operating limits are established for each fuel type present in the core. During operation, each fuel type is monitored against the appropriate operating limits.

Thermal hydraulic characteristics are determined for each fuel type that will be present in the core. The thermal hydraulic characteristics used in core design, safety analysis, and core monitoring are developed on a consistent basis for both AREVA NP fuel and other vendor co-resident fuel to minimize variability due to methods. Geometric data for the co-resident fuel is obtained from the utility, generally under a proprietary agreement. The hydraulic characteristics are based on flow test measurements performed for both AREVA NP fuel and co-resident fuel in the AREVA NP hydraulic flow test facility. For analyses performed to assess core thermal and hydraulic performance with the XCOBRA computer code, each fuel type in the core is explicitly modeled with the appropriate geometric data and hydraulic characteristics.

The GE14 fuel design will be present during the ATRIUM-10 transition cycles at Browns Ferry. A GE14 fuel design was flow tested by AREVA NP in 2002. The GE14 design that will be co-resident with the ATRIUM-10 fuel at Browns Ferry was confirmed to be hydraulically the same as the GE14 assembly tested by AREVA NP.

For core design and nuclear safety analyses, the neutronic cross-section data is developed for each fuel type in the core using CASMO-4. Geometric and nuclear design data (e.g., enrichment distribution) that is required to prepare CASMO-4 input for the co-resident fuel is obtained from the utility, generally under a proprietary agreement. MICROBURN-B2 is used to

design the core and provide input to safety analyses (core neutronic characteristics, power distributions, etc.). Each fuel assembly is explicitly modeled in MICROBURN-B2 using cross-section data from CASMO-4 and geometric data appropriate for the fuel design.

Fuel assembly thermal mechanical limits for both AREVA NP and co-resident fuel are verified and monitored for each mixed core designed by AREVA NP. The thermal mechanical limits established by the co-resident fuel vendor continue to be applicable for mixed (transition) cores. The thermal mechanical limits (steady-state and transient) for the co-resident fuel are provided to AREVA NP by the utility. AREVA NP performs design and licensing analyses to demonstrate that the core design meets steady-state limits and that transient limits are not exceeded during anticipated operational occurrences.

For fast pressurization transients and co-resident GNF fuel, AREVA NP provides transient COTRANSA2/XCOBRA-T surface heat flux benchmark data to the utility. The utility in turn develops corresponding surface heat flux limits and appropriate LHGRFAC values from the COTRANSA2/XCOBRA-T response based on GNF thermal-mechanical analyses. A sufficient number of cases are benchmarked such that a conservative correlation is developed. The process ensures compliance with GNF's thermal-mechanical licensing limits for transient analyses of the co-resident fuel performed with COTRANSA2/XCOBRA-T.

The critical power ratio (CPR) is evaluated for each fuel type in the core using calculated local fluid conditions and an appropriate critical power correlation. Fuel type specific correlation coefficients for AREVA NP fuel are based on data from the AREVA NP critical power test facility. Unless the co-resident fuel critical power correlation is provided to AREVA NP, the AREVA NP critical power correlation is applied to the co-resident fuel. An NRC-approved process for developing correlation coefficients and the associated uncertainty when applying an AREVA NP critical power correlation for co-resident fuel is described in Reference A.2. If adequate test data is available for the co-resident fuel, the correlation coefficients and uncertainty are determined using the process consistent with the approval of the correlation. When test data for the co-resident fuel is not available to AREVA NP, fuel type specific correlation coefficients and uncertainty are developed using calculated CPR data provided by the utility based on an alternate (indirect) approach described in Reference A.2.

The SPCB critical power correlation will be used for monitoring GE14 fuel present during the ATRIUM-10 transition cycles at Browns Ferry. Consistent with the NRC-approved methodology, the indirect approach from Reference A.2 was used to develop correlation coefficients and uncertainty based on CPR data provided to AREVA NP by TVA.

Analyses performed to determine the safety limit MCPR explicitly address mixed core effects. Each fuel type present in the core is explicitly modeled using appropriate geometric data, thermal hydraulic characteristics, and power distribution information (from CASMO-4 and MICROBURN-B2 analyses). CPR is evaluated for each assembly using fuel type specific SPCB correlation coefficients. Plant and fuel type specific uncertainties are considered in the statistical analysis performed to determine the safety limit MCPR. The safety limit MCPR analysis is performed each cycle and uses the cycle specific core configuration.

An operating limit MCPR is established for each fuel type in the core. For fast transients the COTRANSA2 code (Reference A.1) is used to determine the overall system response. The core nuclear characteristics used in COTRANSA2 are obtained from MICROBURN-B2 and reflect the actual core loading pattern. Boundary conditions from COTRANSA2 are used with an XCOBRA-T core model. In the XCOBRA-T model, a hot channel with appropriate geometric and thermal hydraulic characteristics is modeled for each fuel type present in the core. Critical power performance is evaluated using local fluid conditions and fuel type specific CPR correlation coefficients. The transient CPR response is used to establish an operating limit MCPR for each fuel type.

For transient events that are sufficiently slow such that the heat transfer remains in phase with changes in neutron flux during the transient, evaluations are performed with MICROBURN-B2 in accordance with NRC approval. Such slow transients are modeled with the MICROBURN-B2 core simulator code by performing a series of steady state solutions with appropriate boundary conditions using the cycle specific design core loading plan. Each fuel assembly type in the core is explicitly modeled. The change in CPR between the initial and final condition after the transient is determined, and if the CPR change is more severe than those determined from fast transient analyses, the slow transient result is used to determine the MCPR operating limit.

Stability analyses to establish OPRM setpoints and backup stability exclusion regions are performed using the cycle-specific core loading pattern. The stability analyses performed with

RAMONA5-FA and STAIF explicitly model each fuel type in the core. Each fuel type is modeled using appropriate geometric, thermal hydraulic, and nuclear characteristics determined as described above. The stability OPRM setpoints and exclusion region boundaries are established based on the predicted performance of the actual core composition.

MAPLHGR operating limits are established and monitored for each fuel type in the core to ensure that 10 CFR 50.46 acceptance criteria are met during a postulated LOCA. The AREVA NP LOCA methodology is used to establish MAPLHGR limits for AREVA NP fuel. The RELAX code is used to determine the overall system response during a postulated LOCA and provides boundary conditions for a RELAX hot channel model. Each fuel type in the core can be represented by a RELAX hot channel model with appropriate geometric and thermal hydraulic characteristics. Results from the hot channel analysis provide boundary conditions to the HUXY computer code. The HUXY model includes fuel type specific input such as dimensions and local power peaking for each fuel rod.

[

]

[

]

The core monitoring system will monitor each fuel assembly in the core. Each assembly is modeled with geometric, thermal hydraulic, neutronic, and CPR correlation input data appropriate for the specific fuel type. Each assembly in the core will be monitored relative to thermal limits that have been explicitly developed for each fuel type.

In summary, AREVA NP methodology is used consistent with NRC approval to perform design and licensing analyses for mixed cores. The cycle design and licensing analyses explicitly consider each fuel type in mixed core configurations. Co-resident fuel input parameters are developed consistent with the methodology, and in general are developed in the same manner as for AREVA NP fuel. Limits are established for each fuel type and operation within these limits is verified by the monitoring system during operation.

A.2 References

A.1. ANF-913(P)(A) Volume 1 Revision 1 and Volume 1 Supplements 2, 3, and 4, "COTRANSA2: A Computer Program for Boiling Water Reactor Transient Analyses," Advanced Nuclear Fuels Corporation, August 1990.

A.2. EMF-2245(P)(A) Revision 0, "Application of Siemens Power Corporation's Critical Power Correlations to Co-Resident Fuel", Siemens Power Corporation, August 2000.

Appendix B Thermal Hydraulic Methods

B.1 Hydraulic Characterization

The Zuber-Findlay drift flux model (Reference B.1) is utilized in the AREVA NP nuclear and safety analysis methods for predicting vapor void fraction in the BWR system. The model has a generalized form that may be applied to two phase flow by defining an appropriate correlation for the void concentration parameter, Co, and the drift flux, Vgj. The model parameters account for the radially non-uniform distribution of velocity and density and the local relative velocity between the phases, respectively. This model has received broad acceptance in the nuclear industry and has been successfully applied to a host of different applications, geometries, and fluid conditions through the application of different parameter correlations (Reference B.8).

Two different correlations are utilized at AREVA NP to describe the drift flux parameters for the analysis of a BWR core. The correlations and treatment of uncertainties are as follows:

- The nuclear design, frequency domain stability, nuclear AOO transient and accident analysis methods use the [ ] void correlation (Reference B.5) to predict nuclear parameters. Uncertainties are addressed at the overall methodology and application level rather than individually for the individual correlations of each method. The overall uncertainties are determined statistically by comparing predictions using the methods against measured operating data for the reactors operating throughout the world.

- The thermal-hydraulic design, system AOO transient and accident analysis, and loss of coolant accident (only at specified junctions) methods use the Ohkawa-Lahey void correlation (Reference B.6). This correlation is not used in the direct computation of nuclear parameters in any of the methods. Uncertainties are addressed at the overall methodology level through the use of conservative assumptions and biases to assure uncertainties are bounded.

The [ ] void correlation was developed for application to multi-rod geometries operating at typical BWR operating conditions using multi-rod data and was also validated against simple geometry data available in the public domain. The correlation was defined to be functionally dependent on the mass flux, hydraulic diameter, quality, and fluid properties.

The multi-rod database used in the [

]. As a result, the multi-rod database and prediction uncertainties are not available to AREVA NP. However, the correlation has been independently validated by AREVA NP against public domain multi-rod data and proprietary data collected for a prototypical ATRIUM-10 test assembly. Selected results for the ATRIUM-10 test assembly are reported in the public domain in Reference B.9.

The Ohkawa-Lahey void correlation was developed for application in BWR transient calculations. In particular, the correlation was carefully designed to predict the onset of counter current flow limit (CCFL) characteristics during the occurrence of a sudden inlet flow blockage. The correlation was defined to be functionally dependent on the mass flux, quality, and fluid properties.

Independent validation of the correlation was performed by AREVA NP at the request of the NRC during the NRC review of the XCOBRA-T code. The NRC staff subsequently reviewed and approved Reference B.7, which compared the code to a selected test from the FRIGG experiments (Reference B.4). More recently the correlation has been independently validated by AREVA NP against additional public domain multi-rod data and proprietary data collected for a prototypic ATRIUM-10 test assembly.

The characteristics of the AREVA NP multi-rod void fraction validation database are listed in Table B-1.

The FRIGG experiments have been included in the validating database because of the broad industry use of these experiments in benchmarking activities, including TRAC, RETRAN, and S-RELAP5. The experiments include a wide range of pressure, subcooling, and quality from which to validate the general applicability of a void correlation. However, the experiments do not contain features found in modern rod bundles such as part length fuel rods and mixing vane grids. The lack of such features makes the data less useful in validating correlations for modern

fuel designs. Also the reported instrument uncertainty for these tests is provided in Table B-1 based on mockup testing. However, the total uncertainty of the measurements (including power and flow uncertainties) is larger than the indicated values.

Because of its prototypical geometry, the ATRIUM-10 void data collected at KATHY was useful in validating void correlation performance in modern rod bundles that include part length fuel rods, mixing vane grids, and prototypic axial/radial power distributions. Void measurements were made at one of three different elevations in the bundle for each test point: just before the end of the part length fuel rods, midway between the last two spacers, and just before the last spacer.

As shown in Figure B-1, the range of conditions for the ATRIUM-10 void data are valid for typical reactor conditions. This figure compares the equilibrium quality at the plane of measurement for the ATRIUM-10 void data with the exit quality of bundles in the EMF-2158(P)(A) benchmarks and Browns Ferry operating at EPU conditions. As seen in the figure, the data at the measurement plane covers nearly the entire range of reactor conditions. However, calculations of the exit quality from the void tests show the overall test conditions actually envelope the reactor conditions. (Note, the ATRIUM-10 data shown in Figure B-1 is not from the same database as illustrated in Table B-1.)

Figure B-2 and Figure B-3 provide comparisons of predicted versus measured void fractions for the AREVA NP multi-rod void fraction validation database using the [ ] correlation. These figures show the predictions fall within ±0.05 (predicted – measured) error bands with good reliability and with very little bias. Also, there is no observable trend of uncertainty as a function of void fraction.

Figure B-4 and Figure B-5 provide comparisons of predicted versus measured void fractions for the AREVA NP multi-rod void fraction validation database using the Ohkawa-Lahey correlation. In general, the correlation predicts the void data with a scatter of about ±0.05 (predicted – measured), but a bias in the prediction is evident for voids between 0.5 and 0.8. The observed under prediction is consistent with the observations made in Reference B.2.

An extensive validation of the Ohkawa-Lahey void-quality correlation is provided in Reference B.10, which is in addition to the validation performed by AREVA NP. This reference

demonstrates the correlation performance over a very broad range of geometries and flow conditions.

The results reported by the authors demonstrate the correlation has good agreement for all tests except for those tests where the hydraulic diameter is in excess of 0.5 ft (0.152 m). However, the correlation is not applied to geometries of this size in any AREVA NP methodologies.

A measured versus predicted plot of void fraction containing all the data analyzed by the authors (Reference B.10) is reproduced in Figure B-6. The data with hydraulic diameter in excess of 0.5 ft (0.152 m) are indicated as "CARRIER DATA" and "HUGHES (B&W) DATA" in this figure. The statistical results and conclusions reported by the authors for geometries similar to BWR rod bundles are consistent with the AREVA NP assessment reported in this section. One set of data in this population extended above a pressure of [ ], which was reported by Petrick (Reference B.11).

The Petrick data provided experimental results for co-current down-flow at 600, 1000, and 1500 psia (4.1, 6.9, and 10.3 MPa) in a 1.939-inch (0.049 m) diameter tube. The mean and standard deviation of the absolute error (measured-predicted void fraction) for the Ohkawa-Lahey void-quality correlation were reported as 0.038 and 0.050, respectively for the 1500 psia (10.3 MPa) data set in Reference B.10. The reasonable agreement between the data and Ohkawa-Lahey predictions shows the extensibility of the correlation to pressures and flow conditions outside the range experienced in BWR rod bundles under typical operating and transient conditions, including it's extensibility to pressures up to 1500 psia (10.3 MPa).

In summary, the Ohkawa-Lahey void-quality correlation is justified for use above 1000 psia (6.9 MPa) based on validation of the correlation to a broad range of geometries and flow conditions, including pressures up to 1500 psia (10.3 MPa).

The previous discussions justified the applicability of the drift flux correlations for the ATRIUM-10. The same correlations are used for legacy fuel in mixed cores. The geometry and features of the legacy fuel are very similar to the ATRIUM-10, thus the previous discussions are equally applicable to legacy fuel.

In conclusion, validation using the AREVA NP multi-rod void fraction validation database has shown that both drift flux correlations remain valid for modern fuel designs. Furthermore, there is no observable trend of uncertainty as a function of void fraction. This shows there is no increased uncertainty in the prediction of nuclear parameters at EPU (including an extended power/flow operating map) conditions within the nuclear methods as a result of changes to the population distribution of the nodal void fractions with respect to pre EPU conditions.

B.2 References

B.1. N. Zuber and J. A. Findlay, "Average Volumetric Concentration in Two-Phase Flow Systems," J. Heat Transfer, 1965.

B.2. J. Skaug et al., "FT-36b, Results of void Measurements," FRIGG-PM-15, May 1968.

B.3. O. Nylund et al., "Hydrodynamic And Heat Transfer Measurements On A Full-Scale Simulated 36-Rod Marviken Fuel Element With Uniform Heat Flux Distribution," FRIGG-2, R-447/RTL-1007, May 1968.

B.4. O. Nylund et al., "Hydrodynamic and Heat Transfer Measurements on A Full-Scale Simulated 36-Rod Marviken Fuel Element with Non-Uniform Radial Heat Flux Distribution," FRIGG-3, R-494/RL-1154, November 1969.

B.5. [

]

B.6. K. Ohkawa and R. T. Lahey, Jr., "The Analysis of CCFL Using Drift-Flux Models," Nuclear Engineering and Design, 61, 1980.

B.7. XN-NF-84-105(P)(A) Volume 1 Supplement 4, "XCOBRA-T: A Computer Code For BWR Transient Thermal-Hydraulic Core Analysis, Void Fraction Model Comparison to Experimental Data," Advanced Nuclear Fuels Corporation, June 1988.

B.8. P. Coddington and R. Macian, "A Study Of The Performance Of Void Fraction Correlations Used In The Context Of Drift-Flux Two-Phase Flow Models," Nuclear Engineering and Design, 215, 199-216, June 2002.

B.9. S. Misu et al., "The Comprehensive Methodology for Challenging BWR Fuel Assembly and Core Design used at FANP," proceedings on CD-ROM, PHYSOR 2002, Seoul, Korea, October 7-10, 2002

B.10. B. Chexal, et al., "An Assessment of Eight Void Fraction Models for Vertical Flows," NSAC-107, Electric Power Research Institute, December 1986.

B.11. Michael Petrick, "A Study of Vapor Carryunder and Associated Problems," ANL-6581, Argonne National Laboratory, July 1962.

Table B-1 AREVA NP Multi-Rod Void Fraction Validation Database

	FRIGG-2 (Reference B.3)	FRIGG-3 (References B.4 and B.2)	ATRIUM-10-KATHY
Axial Power Shape	uniform	uniform	[ ]
Radial Power Peaking	uniform	mild peaking	[ ]
Bundle Design	circular array with 36 rods + central thimble	circular array with 36 rods + central thimble	prototypic ATRIUM-10 CHF bundle
Pressure (psi)	725	725, 1000, and 1260	[ ]
Inlet Subcooling (^{0}F)	4.3 to 40.3	4.1 to 54.7	[ ]
Mass Flow Rate (lbm/s) *(calculated from mass flux assuming ATRIUM-10 inlet flow area)*	14.3 to 31.0	10.1 to 42.5	[ ]
Equilibrium Quality at Measurement Plane (fraction)	-0.036 to 0.203	-0.058 to 0.330	[ ]
Max Void at Measurement Plane (fraction)	0.828	0.848	[ ]
Reported Instrument Uncertainty (fraction)	0.025	0.016	[ ]
Number of Data	27 tests, 174 points	39 tests, 157 points	[ ]

Figure B-1 Comparison of the Measured Local Quality for ATRIUM-10 Void Data and Exit Quality for Typical Reactor Conditions

Figure B-2 Validation of [ ] using FRIGG-2 and FRIGG-3 Void Data

Figure B-3 Validation of [ ] using ATRIUM-10 Void Data

Figure B-4 Validation of Ohkawa-Lahey using FRIGG-2 and FRIGG-3 Void Data

Figure B-5 Validation of Ohkawa-Lahey using ATRIUM-10 Void Data

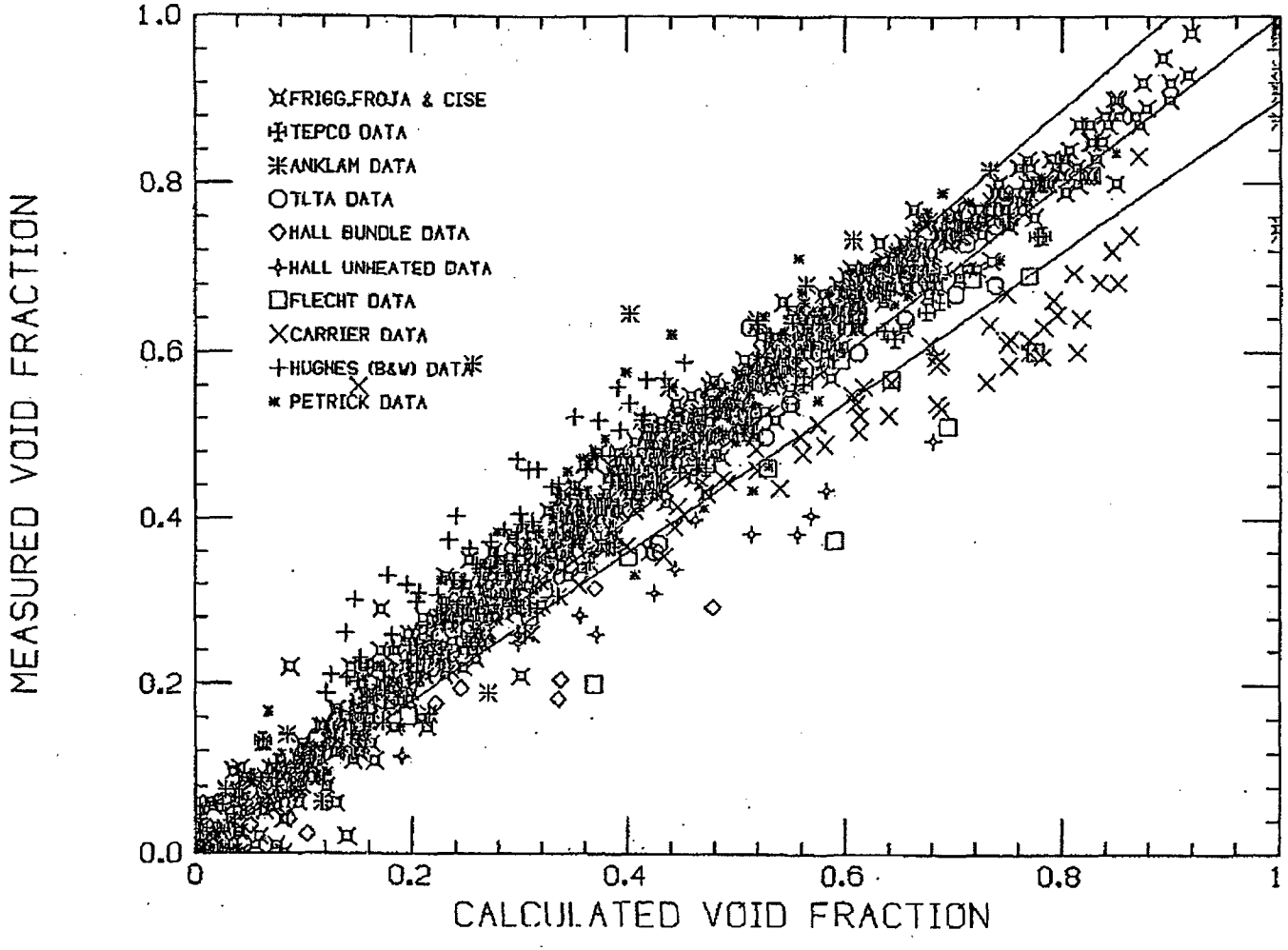

Figure B-6 Measured Versus Calculated Void Fractions

Appendix C Neutronic Methods

C.1 Cross Section Representation

CASMO-4 performs a multi-group [ ] spectrum calculation using a detailed heterogeneous description of the fuel lattice components. Fuel rods, absorber rods, water rods/channels and structural components are modeled explicitly. The library has cross sections for [ ] materials including [ ] heavy metals. Depletion is performed with a predictor-corrector approach in each fuel or absorber rod. The two-dimensional transport solution is based upon the [ ]. The solution provides pin-by-pin power and exposure distributions, homogeneous multi-group (2) micro-scopic cross sections as well as macro-scopic cross sections. Discontinuity factors are determined from the solution. [ ] gamma transport calculation are performed. The code has the ability to perform [ ] calculations with different mesh spacings. Reflector calculations are easily performed.

MICROBURN-B2 performs microscopic fuel depletion on a nodal basis. The neutron diffusion equation is solved with a full two energy group method. A modern nodal method solution using discontinuity factors is used along with a [ ]. The flux discontinuity factors are [ ]. A multilevel iteration technique is employed for efficiency. MICROBURN-B2 treats a total of [ ] heavy metal nuclides to account for the primary reactivity components. Models for nodal [ ] are used to improve the accurate representation of the in-reactor configuration. A full three-dimensional pin power reconstruction method is utilized. TIP (neutron and gamma) and LPRM response models are included to compare calculated and measured instrument responses. Modern steady state thermal hydraulics models define the flow distribution among the assemblies. [ ] based upon CASMO-4 calculations are used for the in-channel fluid conditions as well as in the bypass and water rod regions. Modules for the calculation of CPR, LHGR and MAPLHGR are implemented for direct comparisons to the operating limits.

MICROBURN-B2 determines the nodal macroscopic cross sections by summing the contribution of the various nuclides.

$$\Sigma_x(\rho,\Pi,E,R)=\sum_{i=1}^{I}N_i\sigma_x^i(\rho,\Pi,E,R)+\Delta\Sigma_x^b(\rho,\Pi,E,R)$$

where:

Σ_x	= nodal macroscopic cross section
$\Delta\Sigma_x^b$	= background nodal macroscopic cross section $(D,\Sigma_f,\Sigma_a,\Sigma_r)$
N_i	= nodal number density of nuclide "i"
σ_x^i	= microscopic cross section of nuclide "i"
I	= total number of explicitly modeled nuclides
ρ	= nodal instantaneous coolant density
Π	= nodal spectral history
E	= nodal exposure
R	= control fraction

The functional representations of σ_x^i and $\Delta\Sigma_x^b$ come from 3 void depletion calculations with CASMO-4. Instantaneous branch calculations at alternate conditions of void and control state are also performed. The result is a multi dimensional table of microscopic and macroscopic cross sections that is shown in Figure C-1 and Figure C-2.

At BOL the relationship is fairly simple; the cross section is only a function of void fraction (water density) and the reason for the variation is the change in the spectrum due to the water density variations. At any exposure point, a quadratic fit of the three CASMO-4 data points is used to represent the continuous cross section over instantaneous variation of void or water density. This fit is shown in Figure C-3 and Figure C-4.

Detailed CASMO-4 calculations confirm that a quadratic fit accurately represents the cross sections as shown in Figure C-5, Figure C-6, and Figure C-7.

With depletion the isotopic changes cause other spectral changes. Cross sections change due to the spectrum changes. Cross sections also change due to self shielding as the concentrations change. These are accounted for by the void (spectral) history and exposure parameters. Exposure variations utilize a piecewise linear interpolation over tabulated values at

[ ] exposure points. The four dimensional representation can be reduced to three dimensions (see Figure C-8) by looking at a single exposure.

Quadratic interpolation is performed in each direction independently for the most accurate representation. Considering the case at 70 GWd/MTU with an instantaneous void fraction of 70% and a historical void fraction of 60%, Figure C-9 and Figure C-10 illustrate the interpolation process. The table values from the library at 0, 40 and 80 % void fractions are used to generate 3 quadratic curves representing the behavior of the cross section as a function of the historical void fraction for each of the tabular instantaneous void fractions (0, 40 and 80 %).

The intersection of the three quadratic lines with the historical void fraction of interest are then used to create another quadratic fit in order to obtain the resultant cross section as shown in Figure C-10.

The results of this process for all isotopes and all cross sections in MICROBURN-B2 were compared for an independent CASMO-4 calculation with continuous operation at 20, 60 and 90% void and are presented in Figure C-11. Branch calculations at 90% void from a 40% void depletion were performed for multiple exposures. The results show very good agreement for the whole exposure range as shown in Figure C-12.

At the peak reactivity point, multiple comparisons were made (Figure C-13) to show the results for various instantaneous void fractions.

[

] The errors observed in the figure demonstrate that the errors [ ] are not significantly different from those seen with interpolation. This indicates that the uncertainties in the power distribution determined in EMF-2158(P)(A) are expected to be valid with [ ].

Void fraction has been used for the previous illustrations; however MICROBURN-B2 uses water density rather than void fraction in order to account for pressure changes as well as sub-cooled density changes. This transformation does not change the basic behavior as water density is

proportional to void fraction. MICROBURN-B2 uses spectral history rather than void history in order to account for other spectral influences due to actual core conditions (fuel loading, control rod inventory, leakage, etc.) The Doppler feedback due to the fuel temperature is modeled by accumulating the Doppler broadening of microscopic cross sections of each nuclide.

$$\Delta\Sigma_x = (\sqrt{T_{eff}} - \sqrt{T_{ref}}) \sum_i^I \frac{\partial \sigma_x^i}{\partial \sqrt{T_f}} N_i$$

where:

T_{eff} = Effective Doppler Fuel Temperature
T_{ref} = Reference Doppler Fuel Temperature
σ_x^i = Microscopic Cross Section (fast and thermal absorption) of nuclide "i"
N_i = Density of nuclide "i"

The partial derivatives are determined from branch calculations performed with CASMO-4 at various exposures and void fractions for each void history depletion. The tables of cross sections include data for [ ] states. The process is the same for [ ] states. Other important feedbacks to nodal cross sections are lattice [ ] and instantaneous [ ] between lattices of different [ ]. These feedbacks are modeled in detail.

MICROBURN-B2 versions prior to 2003 treated cross section dependency on spectral history differently between the fuel nuclide depletion module and the neutron flux calculation module. The fuel nuclide depletion module used [ ] while the neutron flux iteration calculation module used a [ ]. This inconsistency was remedied starting from 2003 by changing the depletion module to the [quadratic interpolation/piecewise linear extrapolation on spectral history]. Starting from 2006, both modules were converted to the [ ].

These changes over the years were mainly due to code maintenance concerns and did not impact any result due to the [ ]. Unlike the cross section dependency on the instantaneous void, the [ ] is rather weak. This is shown in Figure C-15 for Pu-239 and in

Figure C-16 for Pu-240. The [

]. At the high end of [ ], the difference between the [

]. This kind of difference is entirely within the uncertainty of nuclear cross section measurement and its evaluation process including the CASMO-4 lattice code. It has no observable effect on the reactor nodal power distribution and the reactor criticality evaluation as has been verified in the code maintenance record of MICROBURN-B2.

CASMO-4 has the capability to specify the density of the moderator in the bypass and in-channel water rods, [ ] the AREVA NP methodology [ ] during operation are not significant. Bypass voiding is not encountered during steady-state EPU operation for Browns Ferry so there is no impact on steady-state analyses. For transient conditions it is conservative to ignore the density changes as additional voiding aids in shutting down the power generation.

The methods used in CASMO-4 are state of the art. The methods used in MICROBURN-B2 are state of the art. The methodology accurately models a wide range of thermal hydraulic conditions including EPU and extended power/flow operating map conditions.

C.2 Applicability of Uncertainties

The EMF-2158(P)(A) data was re-evaluated by looking at the deviations between measured and calculated TIP response for each axial level. The standard deviation of these deviations at each axial plane are presented in Figure C-17 and demonstrate that there is no significant trend vs. axial position, which indicates no significant trend vs. void fraction.

Bundle gamma scan data is not used directly to define the calculated bundle power distribution uncertainty. Gamma scan data is used to define the correlation coefficients as described in EMF-2158(P) (A) "Siemens Power Corporation Methodology for Boiling Water Reactors: Evaluation and Validation of CASMO-4 Microburn-B2". Both TIP uncertainties and these correlation coefficients are used to calculate the bundle power distribution uncertainty. The

correlation coefficient is determined from comparison of the calculated power distribution to available bundle gamma scan data.

The TIPs directly measure the local neutron flux from the surrounding four fuel assemblies. Thus, the calculated bundle power distribution uncertainty will be closely related to the calculated TIP uncertainty. However, the bundle powers in the assemblies surrounding a TIP are not independent. If a bundle is higher in power, neutronic feedback increases the power in the nearby assemblies, thus producing a positive correlation between nearby bundles. The gamma scan data provides the means to determine this correlation according to the EMF-2158(P)(A) methodology. A smaller correlation coefficient implies that there is less correlation between nearby bundle powers, thus, there would be a larger bundle power distribution uncertainty.

To compare core physics models to the gamma scan results, the calculated pin power distribution is converted into a Ba140 density distribution. A rigorous mathematical process using CASMO-4 pin nuclide inventory and MICROBURN-B2 nodal nuclide inventory is used.

Gamma scan comparisons for 9X9-1 and ATRIUM-10 fuel were presented in the topical report, EMF-2158(P)(A), in Section 8.2.2. Figures 8.18 through 8.31 showed very good comparisons between the calculated and measured relative Ba-140 density distributions for both radial and axial values.

The Quad Cities assembly gamma scan data was used to determine the correlation coefficient which accounts for the correspondence between the assembly powers of adjacent assemblies. This correspondence is quantified by a conservative multiplier to the uncertainty in the TIP measurements. In order to conservatively account for this correspondence, the bundle power uncertainty is increased due to the radial TIP uncertainty by a multiplier based on the correlation coefficient. The correlation coefficient is statistically calculated and shown in Figure 9.1 and Figure 9.2 of EMF-2158(P)(A). It indicates a less than perfect correlation between powers of neighboring bundles. The conservative multiplier is calculated as follows:

[ ]

The calculated TIP uncertainty would normally be expected to be slightly larger than the calculated power uncertainty due to the TIP model. The Quad Cities gamma scan comparison shows the 2-D radial power uncertainty of [ ] (see Section 9.6 of EMF-2158(P)(A)). The D-Lattice plant calculated radial TIP uncertainty is [ ]. The data indicates that the calculated TIP uncertainty is indeed larger than the calculated power uncertainty. The use of the correlation coefficient to increase the calculated power uncertainty is a very conservative approach resulting from the statistical treatment. The types of fuel bundles (8x8, 9x9, or 10x10) loaded in the core has no effect on the reality of the physical model which precludes the possibility of the calculated power uncertainty to be larger than the calculated TIP uncertainty. The accuracy of the MICROBURN-B2 models is demonstrated by comparisons between measured and calculated TIP's as well as comparison of calculated and measured Lanthanum-140 activation. The accuracy of the MICROBURN-B2 models was further validated with detailed axial pin by pin gamma scan measurements of 9X9-1 and ATRIUM-10 fuel assemblies in the reactor designated as KWU-S. These measurements demonstrated the continued accuracy of the MICROBURN-B2 models with modern fuel assemblies. Details of these measurements are provided in Section 8.2.2 of the topical report, EMF-2158(P)(A).

The AREVA NP SLMCPR methodology is used to determine what Technical Specification (TS) SLMCPR value is required to meet the regulatory acceptance criterion (< 0.1% of the rods in the core in BT). The first step in the calculation procedure is to select a value for SLMCPR to two decimal places (usually the current TS SLMCPR). The SAFLIM2 computer code is then used to calculate the number of rods in BT for the selected SLMCPR. If the calculated rods in BT is <0.1%, the selected SLMCPR is supported. If the acceptance criterion is not met, the SLMCPR is increased by 0.01 and the SAFLIM2 calculation is performed again. This iteration is continued until the acceptance criterion is met for the input SLMCPR.

The AREVA NP SAFLIM2 code is used to calculate the number of expected rods in boiling transition (BT) for a specified value of the SLMCPR (i.e., SLMCPR is an input, not a calculated

result). The extremes of the two correlation coefficients from the Quad Cities assembly gamma scan data sets [ ] were used for a sensitivity study of the MCPR safety limit. An analysis of the safety limit was performed with SAFLIM2 using an input SLMCPR of 1.08 and the base RPF uncertainty [ ]. The number of boiling transition (BT) rods was calculated to be 60 from this analysis. The analysis was repeated in a series of SAFLIM2 calculations using the increased RPF uncertainty [ ] and performed by iterating on the input value of SLMCPR. Different values for the SLMCPR input were used until the number of BT rods calculated by SAFLIM2 was the same as the base case (60 rods). A SLMCPR input value of [ ] resulted in 60 rods in BT when the increased RPF uncertainty was input. The difference in SLMCPR input [ ] for the two cases that resulted in the same number of BT rods is a measure of the safety limit sensitivity to the increased RPF uncertainty.

The only input parameters that changed between the two SAFLIM2 analyses were the SLMCPR and the RPF uncertainty. For each analysis, 1000 Monte Carlo trials were performed. To minimize statistical variations in the sensitivity study, the same random number seed was used and all bundles were analyzed for both analyses. As discussed above, 60 rods were calculated to be in BT in both analyses.

This sensitivity study was performed to quantify the sensitivity of SLMCPR to an increase in RPF uncertainty and did not follow the standard approach used in SLMCPR licensing analyses. In standard licensing calculations, the SLMCPR is not input at a precision greater than the hundredths decimal place. As a result, the increased RPF uncertainty would result [ ] [ ] in SLMCPR licensing analyses depending on how close the case was to the acceptance criterion prior to the increase in RPF uncertainty.

The EMF-2158(P)(A) data was also re-evaluated by looking at the deviations between measured and calculated TIP response for each axial level. The standard deviation of these deviations at each axial plane are presented in Figure C-17 and demonstrate that there is no significant trend vs. axial position, which indicates no significant trend vs. void fraction.

Gamma scanning provides data on the relative gamma flux from the particular spectrum associated with La140 gamma activity. The relative gamma flux corresponds to the relative La140 concentration. Based upon the time of shutdown and the time of the gamma scan the Ba140 relative distribution at the time of shutdown is determined. This Ba140 relative

distribution is thus correlated to the pin or assembly power during the last few weeks of operation. The data presented in the topical report, EMF-2158(P)(A), includes both pin and assembly Ba140 relative density data. The assembly gamma scan data was taken at Quad Cities after the operation of cycles 2, 3 and 4. Some of this data also included individual pin data. This data was from 7X7 and 8X8 fuel types. Additional fuel pin gamma scan data was taken at the Gundremingen plant for ATRIUM-9 and ATRIUM-10 fuel. This data is also presented in the topical report.

Pin-by-pin Gamma scan data is used for verification of the local peaking factor uncertainty. The pin gamma scan data from Quad Cities was taken at seven axial levels and resulted in a pin power distribution uncertainty of [ ]. Additional pin gamma scans were taken by KWU at 4 axial levels and included two 9X9 UO_2, one 9X9 MOX and one ATRIUM-10 UO_2 assemblies. The local power uncertainty from the KWU data was [ ] which is very consistent with the Quad Cities data. The consistency of these very different sets of data indicates that additional gamma scan data would not change the uncertainty significantly.

Quad Cities measurements presented in the topical report EMF-2158(P)(A) have been re-evaluated to determine any axial dependency. Figure C-18 presents the raw data including measurement uncertainty and demonstrates that there is no axial dependency. The more recent Gamma scans performed by KWU, presented in the topical report EMF-2158(P)(A) and re-arranged by axial level in Table C-1, indicate no axial dependency. Full axial scans were performed on 16 fuel rods. Comparisons to calculated data show excellent agreement at all axial levels. The dip in power associated with spacers, observed in the measured data, is not modeled in MICROBURN-B2. There is no indication of reduced accuracy at the higher void fractions.

CASMO-4 and MCNP calculations have been performed to compare the fission rate distribution statistics to Table 2-1 of the topical report EMF-2158(P)(A) which is shown in Table C-2. The fission rate differences at various void fractions demonstrate that CASMO-4 calculations have very similar uncertainties relative to the MCNP results for all void fractions. The maximum expected void fraction anticipated for EPU operation is not expected to exceed the void fractions observed in the topical report benchmark. These fission rate differences also meet the criteria of the topical report EMF-2158(P)(A) for all void fractions.

A sensitivity study was performed per a typical BWR to evaluate the impact of local power uncertainty on the calculated MCPR Safety Limit. [

]

Data presented in these figures and tables demonstrate that the AREVA NP methodology is capable of accurately predicting reactor conditions for fuel designs operated under the current operating strategies and core conditions. The uncertainties determined in Reference C.2 are applicable to Browns Ferry Unit 1.

C.3 Fuel Cycle Comparisons

AREVA NP has reviewed the data presented in EMF-2158(P)(A) with regard to the maximum assembly power (Figure C-19) and maximum exit void fraction (Figure C-20) to determine the range of data previously benchmarked.

Fuel loading patterns and operating control rod patterns are constrained by the minimum critical power ratio (MCPR) limit, which consequently limits the assembly power and exit void fraction regardless of the core power level. Operating data from several recent fuel cycle designs has been evaluated and compared to that in the topical report EMF-2158(P)(A). Maximum assembly power and maximum void fraction are presented in Figure C-21 and Figure C-22.

In order to evaluate some of the details of the void distribution a current design calculation was reviewed in more detail. Figure C-23 and Figure C-24 present the following parameters at the point of the highest exit void fraction (at 9336 MWd/MTU cycle exposure) in cycle core design for a BWR6 with ATRIUM-10 fuel. Another measure of the thermal hydraulic conditions is the population distribution of the void fractions. These are representative figures for a high power density plant.

- Core average void axial profile
- Axial void profile of the peak assembly
- Histogram of the nodal void fractions in core

The actual core designs used for each cycle will have slightly different power distributions and reactivity characteristics than any other cycle. Conclusions from analyses that are dependent on the core design (loading pattern, control rod patterns, fuel types) are re-confirmed as part of the reload licensing analyses performed each cycle. Cycle-specific reload licensing calculations will continue to be performed for all future EPU cycles using NRC approved methodologies consistent with the current processes.

Browns Ferry operating under EPU conditions (Figure C-25 and Figure C-26) can be compared to the equivalent data of the topical report EMF-2158(P)(A). Comparison of Figure C-19 vs. Figure C-25 and Figure C-20 vs. Figure C-26 shows that EPU operation in the standard power/flow map is within the range of the original methodology approval for assembly power and exit void fraction. From a neutronic perspective, moderator density (void fraction) and exposure cause the greatest variation in cross sections. NRC-approved exposure limits for ATRIUM-10 fuel evaluated with AREVA NP methods are unchanged for EPU conditions. Reactor conditions for Browns Ferry with power uprate are not significantly different from that of current experience and are bounded by the experience for the important parameters.

The axial profile of the power and void fraction of the limiting assembly and core average values are presented in Figure C-27 for a Browns Ferry EPU cycle design. These profiles demonstrate that the core average void fraction and the maximum assembly power void fractions are bounded by the topical report data and are consistent with recent experience on other reactors.

Figure C-28 presents a histogram of the void fraction for EPU conditions. This histogram was taken at the point of maximum exit void fraction expected during the cycle. The distribution of voids is shifted slightly toward the 70 to 80 % void fraction levels. The population of nodes experiencing 85 to 90% voids is still small.

The neutronic and thermal hydraulic conditions predicted for the EPU operation are bounded by the data provided in the topical report EMF-2158(P)(A) so the isotopic validation continues to be applicable to EPU operation.

The AREVA NP methodology [ ] the reactivity coefficients that are used in the transient analysis. Conservatisms in the methodology are used to produce conservative results that bound the uncertainties in the reactivity coefficients. Data

presented in these referenced figures indicate that there are no significant differences between EPU and non-EPU conditions that have an impact on the reactivity coefficients.

C.3.1 Bypass Voiding

The core bypass water is modeled in the AREVA NP steady-state core simulator, transient simulator, LOCA and stability codes as [ ].

The steady-state core simulator, MICROBURN-B2, explicitly models the assembly specific flow paths through the lower tie-plate flow holes and the channel seals in addition to a [ ] through the core support plate. The numerical solution for the individual flow paths is computed based on a general parallel channel hydraulic solution that imposes a constant pressure drop across the core fuel assemblies and the bypass region. This solution scheme incorporates [ ] that is dependent on the [ ].

The MICROBURN-B2 state-point specific solution for bypass flow rate and [ ] is then used as initial conditions in the transient and LOCA analyses. When the reactor operates on high rod-lines at low flow conditions, the in-channel pressure drop decreases to a point where a solid column of water cannot be supported in the bypass region, and voiding occurs in the core bypass. For these conditions (in the region of core stability concerns) the neutronic feedback of bypass voiding [

]

[

]

The level of bypass boiling for a given state-point is a direct result of the hydraulic solution. The potential for boiling increases as the power/flow ratio increases or the inlet sub-cooling decreases. While the licensing methodology utilizes a [

] to estimate the potential for localized bypass boiling. This [

] to specifically determine a bounding local void distribution in the core. The model is conservative in that it [

]. The capability of this model to predict localized bypass boiling is demonstrated in Figure C-29 for a hypothetical case where the inlet sub-cooling was artificially decreased to induce bypass boiling.

Bypass voiding is of greatest concern for stability analysis due to its direct impact on the fuel channel flow rates and the axial power distributions. The reduced density head in the core bypass due to boiling results in a higher bypass flow rate and consequently a lower hot channel flow rate. This lower hot channel flow rate and a more bottom-peaked power distribution (due to lower reactivity in the top of the core due to boiling in the bypass region) destabilize the core through higher channel decay ratios. AREVA NP stability methods directly model these phenomena to assure that the core stability is accurately predicted.

CASMO-4 has the capability to specify the density of the moderator in the bypass and in-channel water rods, [

].

Bypass voiding is not encountered during full power, steady-state EPU operation for Browns Ferry so there is no impact on steady-state analyses. For transient conditions it is conservative to ignore the density changes as additional voiding aids in shutting down the power generation.

For Browns Ferry, a 100% power / 100% flow statepoint (120% of the original licensed thermal power) was assessed. Even with the conservative multi-channel model, there was no localized

bypass boiling at the EPU power level. This assessment assures that the limiting transients at the uprated thermal power are not adversely affected by bypass boiling. As the flow is reduced along the 100% power line, the decrease in flow is compensated by increased sub-cooling which more than compensates for the decrease in flow. When flow is further reduced along the highest rod line, boiling in the bypass is calculated to begin. This is in the area of stability concerns where the boiling in the bypass is modeled explicitly. For normal operation at 100% power boiling in the bypass is not expected to occur, so there is no impact on the lattice local peaking or the LPRM response.

C.3.2 Fuel Assembly Design

No fuel design modifications have been made for EPU operation, neither mechanical nor thermal hydraulic. The maximum allowed enrichment level of any fuel pellet is 4.95 wt% U-235. A description of fuel enrichments on both a lattice basis and an assembly basis for the first reload of ATRIUM-10 fuel in Browns Ferry is provided in Table C-3.

All new and spent fuel at Browns Ferry is stored in the Spent Fuel Storage Pool (SFSP) and in accordance with Technical Specifications must maintain a subcritical multiplication factor (keff) of less than 0.95 when flooded with non-borated water. A SFSP criticality analysis has been performed for Browns Ferry that confirms that this requirement is met for ATRIUM-10 fuel designs. A reload specific evaluation is performed to verify that the specific bundle designs being loaded remain bounded by the criticality analysis.

C.4 References

C.1 XN-NF-85-67(P)(A) Revision 1, "Generic Mechanical Design for Exxon Nuclear Jet Pump BWR Reload Fuel," Exxon Nuclear Company, September 1986.

C.2 EMF-2158(P)(A), "Siemens Power Corporation Methodology for Boiling Water Reactors: Evaluations and Violation of CASMO-4/MICROBURN-B2," Siemens Power Corporation, October 1999.

Table C-1 KWU-S Gamma Scan Benchmark Results from EMF-2158(P)(A)

Table C-2 Comparison of CASMO-4 and MCNP results for ATRIUM-10 Design

Table C-3 Fuel Enrichment Description for the Initial Browns Ferry Unit 1 EPU ATRIUM-10 Fuel Cycle Design

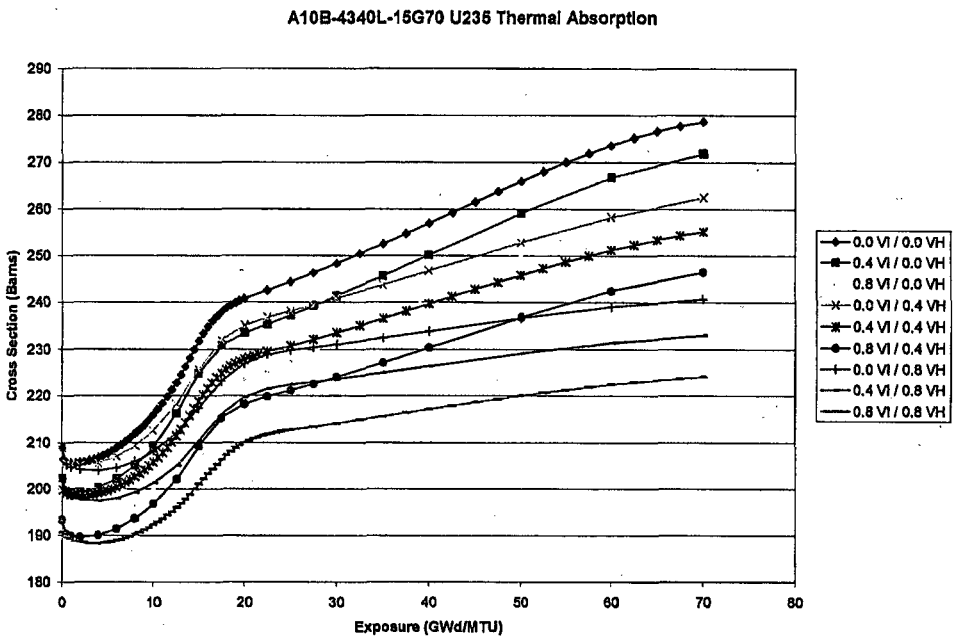

Figure C-1 Microscopic Thermal Cross Section of U-235 from Base Depletion and Branches

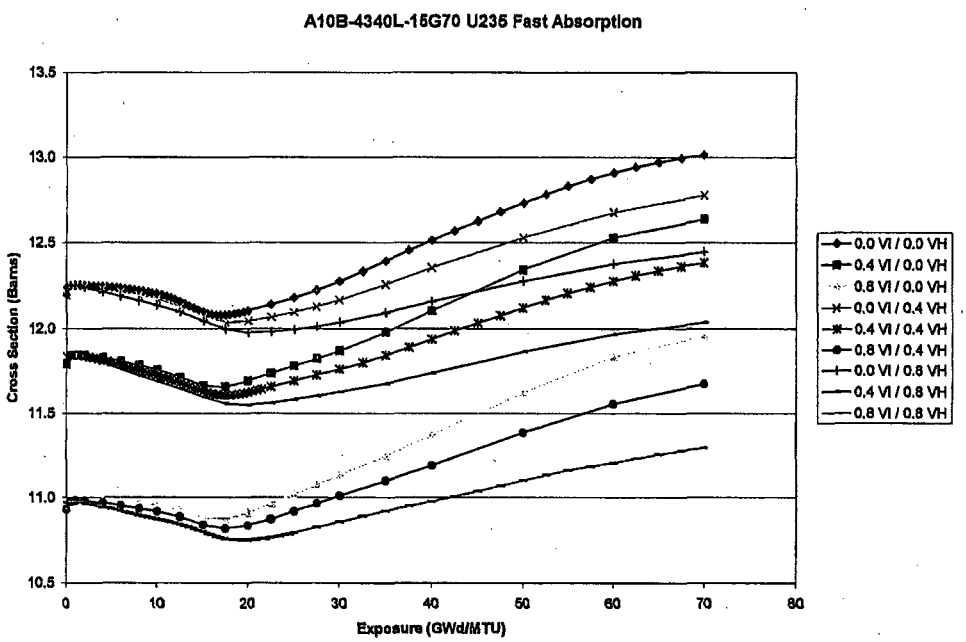

Figure C-2 Microscopic Fast Cross Section of U-235 from Base Depletion and Branches

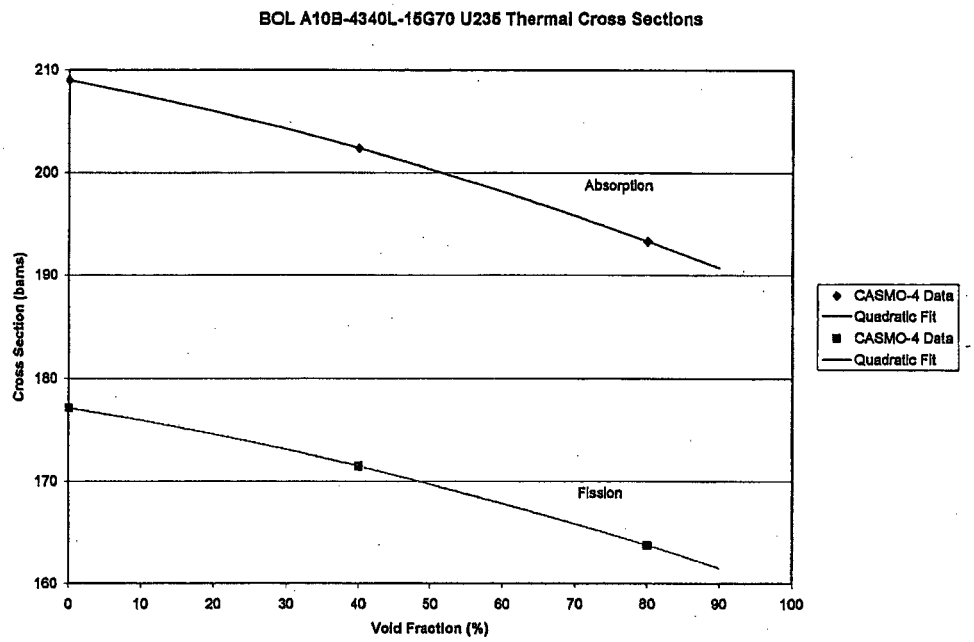

Figure C-3 Microscopic Thermal Cross Section of U-235 at Beginning of Life

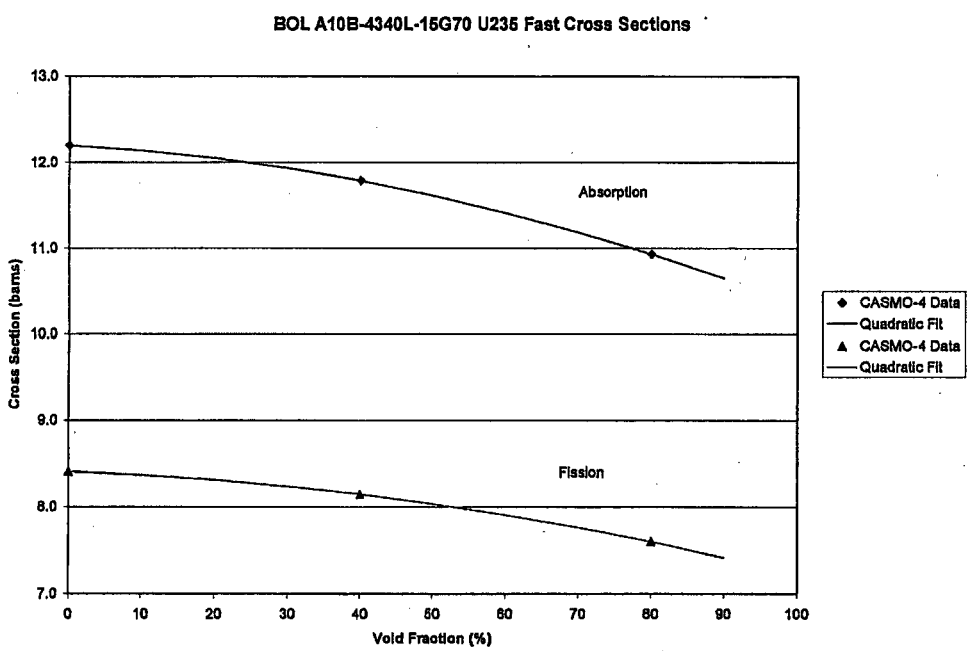

Figure C-4 Microscopic Fast Cross Section of U-235 at Beginning of Life

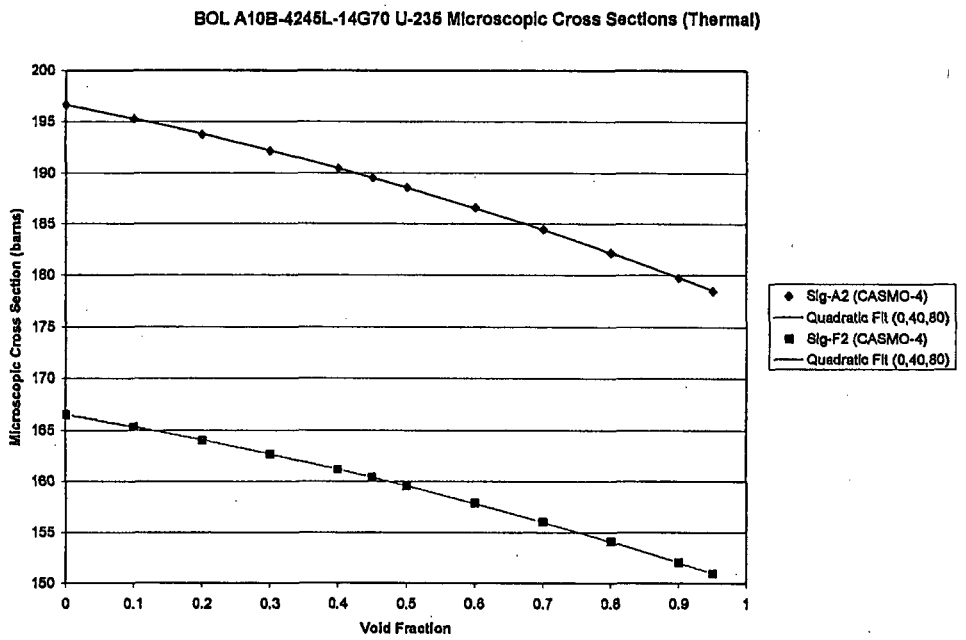

Figure C-5 Microscopic Thermal Cross Section of U-235 Comparison of Quadratic Fit with Explicit Calculations at Various Void Fractions

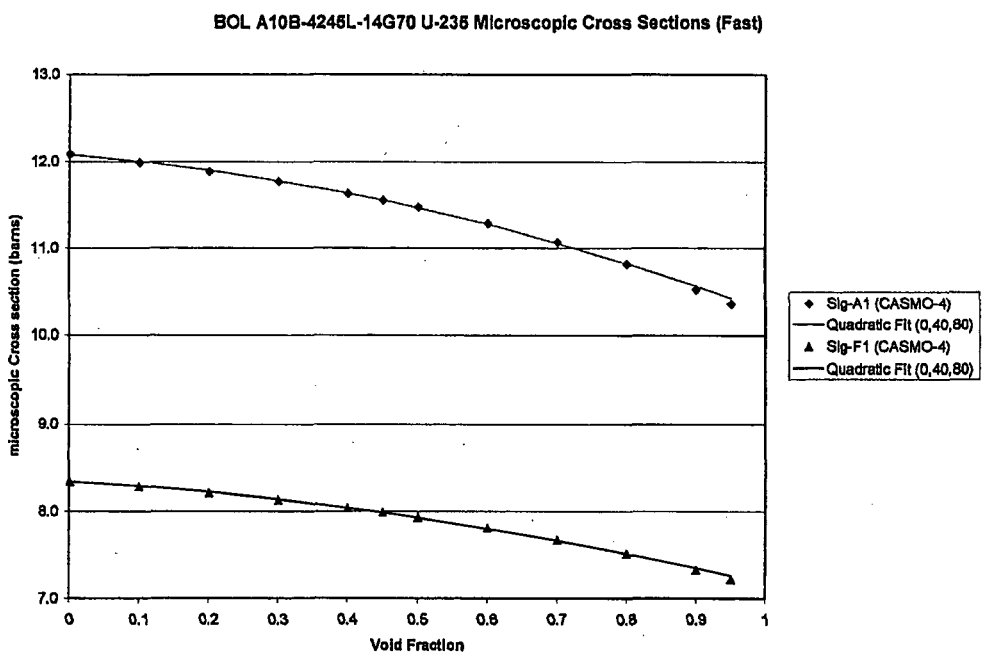

Figure C-6 Microscopic Fast Cross Section of U-235 Comparison of Quadratic Fit with Explicit Calculations at Various Void Fractions

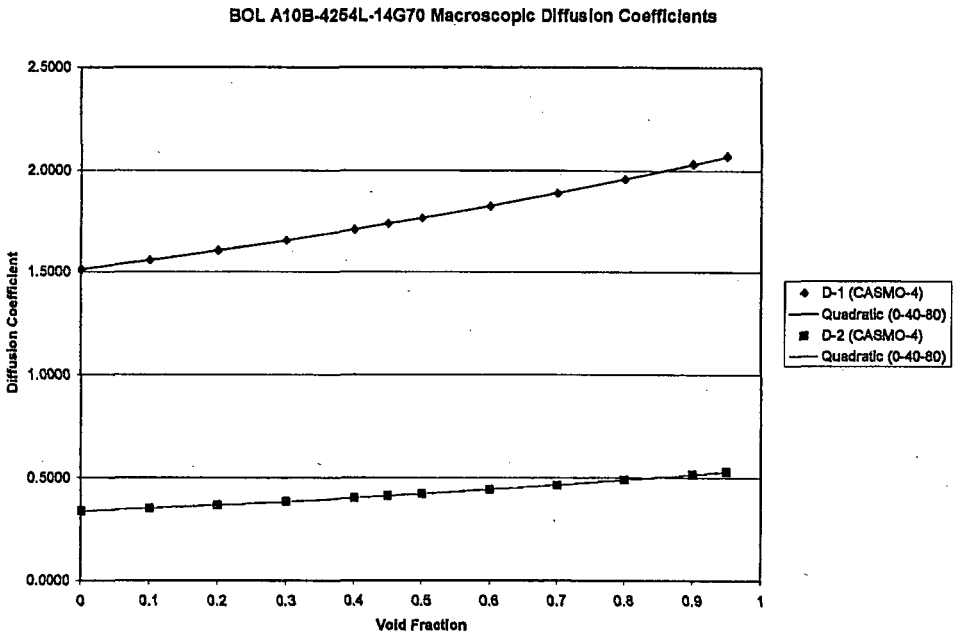

Figure C-7 Macroscopic Diffusion Coefficient (Fast and Thermal) Comparison of Quadratic Fit with Explicit Calculations at Various Void Fractions

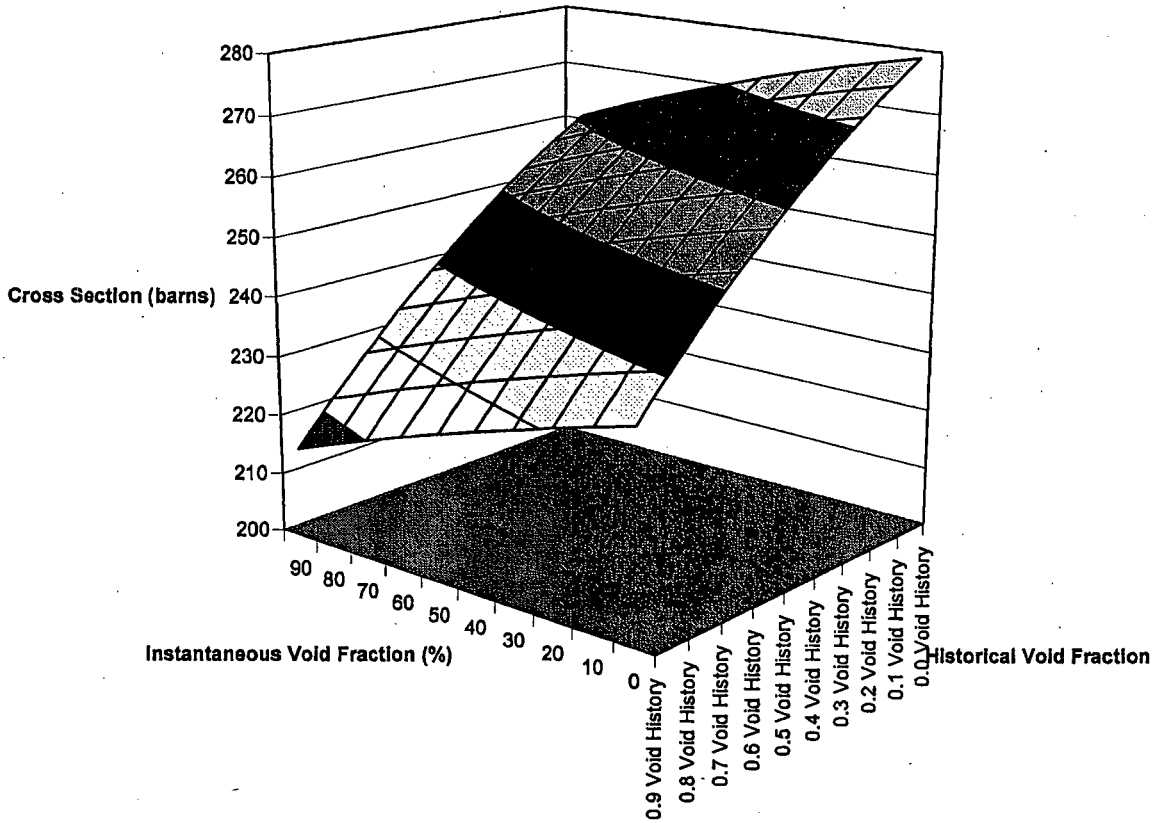

Figure C-8 Microscopic Thermal Cross Section of U-235 at 70 GWd/MTU

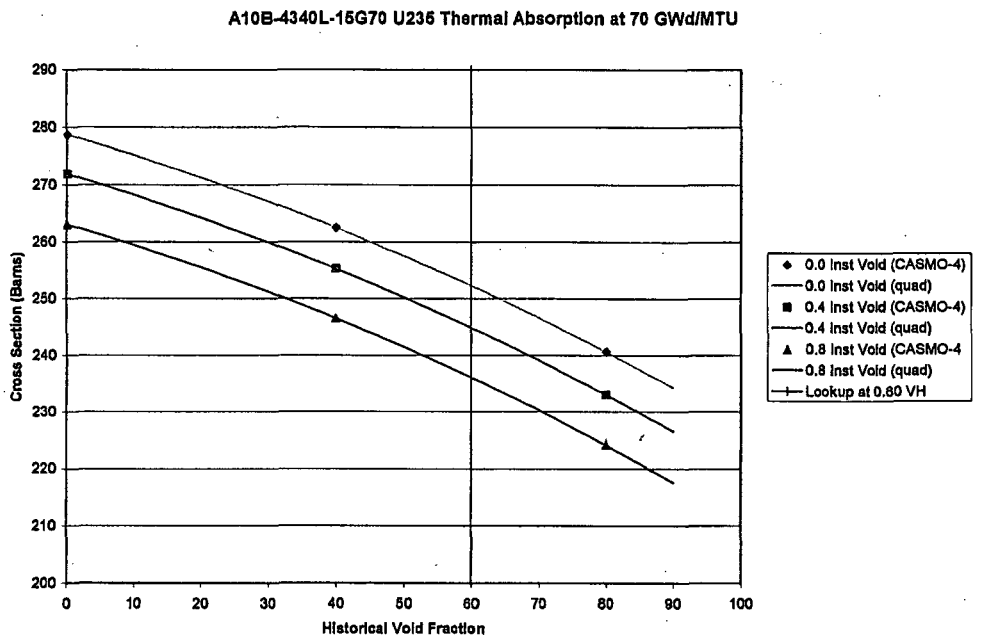

Figure C-9 Quadratic Interpolation Illustration of Microscopic Thermal Cross Section of U-235

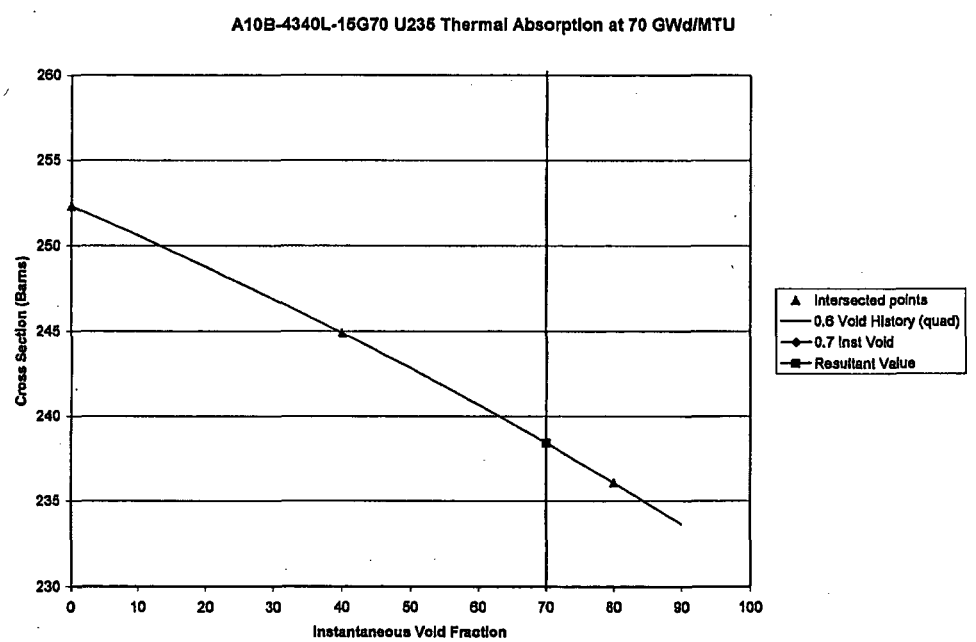

Figure C-10 Illustration of Final Quadratic Interpolation for Microscopic Thermal Cross Section of U-235

Figure C-11 Comparison of k-infinity from MICROBURN-B2 Interpolation Process with CASMO-4 Calculations at Intermediate Void Fractions of 0.2, 0.6 and 0.9

Figure C-12 Comparison of k-infinity from MICROBURN-B2 Interpolation Process with CASMO-4 Calculations at 0.4 Historical Void Fractions and 0.9 Instantaneous Void Fraction

Figure C-13 Delta k-infinity from MICROBURN-B2 Interpolation Process with CASMO-4 Calculations at 0.4 Historical Void Fraction and 0.9 Instantaneous Void Fraction

Figure C-14 Comparison of Interpolation Process Using Void Fractions of 0.0, 0.4 and 0.8 and Void Fractions of 0.0, 0.45 and 0.9

Figure C-15 PU-239 sigma-1 Dependence on Spectral History at 20 GWd/T

Figure C-16 PU-240 sigma-1 Dependence on Spectral History at 20 GWd/T

Figure C-17 EMF-2158(P)(A) TIP Statistics by Axial Level

Figure C-18 Quad Cities Unit 1 Pin by Pin Gamma Scan Results

Figure C-19 Maximum Assembly Power in Topical Report EMF-2158(P)(A)

Figure C-20 Maximum Exit Void Fraction in Topical Report EMF-2158(P)(A)

Figure C-21 Maximum Assembly Power Observed from Recent Operating Experience

Figure C-22 Void Fractions Observed from Recent Operating Experience

Figure C-23 Axial Power and Void Profile Observed from Recent Design Experience

Figure C-24 Nodal Void Fraction Histogram Observed from Recent Design Experience

Figure C-25 Maximum Assembly Power in an EPU Browns Ferry Design

Figure C-26 Maximum Exit Void Fraction in an EPU Browns Ferry Design

Figure C-27 Browns Ferry EPU Design Axial Profile of Power and Void Fraction

Figure C-28 Browns Ferry EPU Design Nodal Void Fraction Histogram

EDIT OF VOID FRACTION IN BYPASS CHANNEL IN UNITS OF %

Figure C-29 Hypothetical MICROBURN-B2 Multi-Channel Average Bypass Void Distribution

Appendix D Stability Methods

D.1 DIVOM Analysis

The DIVOM (Delta over Initial CPR Versus Oscillation Magnitude) for Option III plants was initially defined as a constant regional oscillation mode slope of 0.45 in Licensing Topical Report NEDO-32465-A. An earlier 10 CFR part 21 report (MFN-01-046 dated August 31, 2001) determined that this generic slope may not bound all current core and fuel designs. Closure of this part 21 was accomplished with the implementation of plant/cycle-specific DIVOM calculations as discussed in BWR Owners Group communications BWROG-03047 and -03048. The basis of these calculations is the BWR Owner's Group guideline, GE-NE-0000-0031-6498-R0 transmitted by OG04-0153-260 "Plant-Specific Regional Mode DIVOM Procedure Guideline" dated June 15, 2004. This guideline was later revised in OG05-0136-260 on June 2, 2005. All Browns Ferry DIVOM calculations that were performed are consistent with the latest guideline.

It is important to understand that variations in DIVOM response on a cycle specific basis does not impact safety margin. The purpose of the Option III system is to protect the Technical Specification MCPR Safety Limit if a diverging oscillation event were to be experienced. A cycle specific setpoint calculation is performed to ensure that cycle specific variations in parameters that have the potential to impact the protection of the MCPR Safety Limit are explicitly included. The part 21 documented in MFN-01-046 and its associated closure essentially redefined DIVOM as one of these parameters that need to be calculated on a cycle-specific basis.

An increase in DIVOM slope value for a specific operating cycle does not mean that the core is less stable or more likely to experience an oscillation. A larger DIVOM slope value does mean that the MCPR response for a specified oscillation magnitude is larger. However, since the larger cycle-specific DIVOM value is explicitly included in the setpoint calculation, no degradation in the margin of safety occurs.

D.2 ATWS/Instability

The industry assessments of ATWS rules relative to BWR core thermal-hydraulic stability presented in NEDO-32047-A (Reference D.1) and the mitigation of BWR core thermal-hydraulic

instabilities in ATWS (NEDO-32164) were performed for the BWROG using GNF proprietary codes and methods. These assessments provide strong evidence that the proposed plant operating guideline change to mitigate the instabilities is effective and reduce the consequences of the event. The NRC recognized in its evaluation of (Reference D.2) that these calculations exhibited a high degree of uncertainty, but considered that even if the calculated power oscillation amplitude were in error by an order of magnitude, the conclusions would remain applicable. Therefore, the concern with respect to the core power distributions for EPU cycles loaded with ATRIUM-10 fuel must be assessed relative to this licensing conclusion (within a factor of 10). Since the dynamics of large amplitude limit cycles are only weakly fuel type dependent, due to the enrichment limits and hydraulic compatibility, the analysis of instabilities in the presence of ATWS conditions has been considered a plant analysis. This view is reinforced by the fact that the only effective mitigating action was a plant operating procedure and not a fuel design or cycle design change. Regardless, a brief discussion of the ATWS/Instability issue has been prepared based on a first principles understanding of the instability phenomena, to provide clarification of the phenomena associated with the underlying instability.

D.2.1 Background

The limiting ATWS transient is a turbine trip with 100% bypass which brings the core to natural circulation at a high rod line accompanied by high inlet subcooling. Calculations by GE using TRACG code (Reference D.1) indicate that oscillations can grow to large amplitudes and the global mode is more limiting than the regional mode oscillations. Short prompt-critical pulses were also observed resulting in irregular oscillation peak sequences. The origin of the irregular nature of the peaks was not understood at the time of the review and was attributed to numerical sensitivities leading to the NRC accepting the results with large uncertainties or rather on a qualitative basis. In using this original approved analysis as a discussion basis, it is recognized that the following are the important phenomena:

- Maximum amplitude of the oscillation (limit cycle)
- Average power increase due to the oscillation
- Limiting mode
- Role of the prompt-critical pulses

- Role of void-reactivity coefficient

Based on the phenomenological discussion of the above effects, the consequences of EPU operation and ATRIUM-10 fuel loading will be put in perspective regarding the potential for fuel damage as a consequence of the limiting ATWS transient with instability.

D.2.2 Review of the Important Phenomena

D.2.2.1 Global Oscillation Limit Cycle Amplitude

[

]

[

]

D.2.2.2 Average Power Increase due to Oscillations

[

]

[

]

D.2.2.3 Limiting Mode

[

]

D.2.2.4 The Role of the Prompt-Critical Pulses

[

]

[

]

D.2.2.5 The Role of Void-Reactivity Coefficient

[

]

D.2.3 Assessing the Change in Fuel Damage Potential

The assessment of the fuel damage potential is made with regard to variations related to the ATRIUM-10 fuel type and EPU.

D.2.3.1 Effect of the ATRIUM-10 Fuel Type

The fuel types manufactured by different vendors vary in their respective mechanical design and geometry. However, the variations in the essential operational characteristics such as pressure drop and void-reactivity coefficient are relatively small as necessitated by the need for compatibility in mixed core situations. These variations are not sufficiently large as to affect the nature of a qualitative analysis such as ATWS with instability. No other significant ATWS/Instability phenomena can be related directly to fuel properties.

D.2.3.2 Effect of EPU Core Loading

[

]

[

]

D.3 References

D.1. NEDO-32047-A, "ATWS Rule Issues Relative to BWR Core Thermal-Hydraulic Stability," GE Nuclear Energy, June 1995.

D.2. W. Wolf et al., "BWR Stability Analysis with the BNL Engineering Plant Analyzer," NUREG/CR-5816, October 1992.

D.3. Y. M. Farawila and D. W. Pruitt, "A Study of Nonlinear Oscillations and Limit Cycles in Boiling Water Reactors – I: The Global Mode," Nuclear Science and Engineering: 154, 302-315 (2006).